

Dark matter direct detection rate in a generic model with micrOMEGAs_{2.2} .

G. Bélanger¹, F. Boudjema¹, A. Pukhov², A. Semenov³

1) *Laboratoire de Physique Théorique LAPTH, CNRS, Univ. de Savoie, B.P.110, F-74941 Annecy-le-Vieux Cedex, France*

2) *Skobeltsyn Inst. of Nuclear Physics, Moscow State Univ., Moscow 119991, Russia*

3) *Joint Institute for Nuclear Research (JINR), 141980, Dubna, Russia*

December 15, 2008

Abstract

We present a new module of the micrOMEGAs package for the calculation of WIMP-nuclei elastic scattering cross sections relevant for the direct detection of dark matter through its interaction with nuclei in a large detector. With this new module, the computation of the direct detection rate is performed automatically for a generic model of new physics which contains a WIMP candidate. This model needs to be implemented within micrOMEGAs 2.2.

1 Introduction

The existence of an important cold dark matter (CDM) component has been firmly established by cosmological observations in the last few years notably by SDSS [1] and WMAP [2]. A leading candidate for CDM is a new weakly interacting massive particle (WIMP). This WIMP must be stable. Such particles arise naturally in many extensions of the standard model [3] from the minimal supersymmetric standard model [4, 5] to models of extra dimensions [6, 7, 8, 9], little Higgs models [10] or models with extended gauge [11, 12] or Higgs sectors [13, 14]. In these models the dark matter (DM) candidate can be either a Majorana fermion, a Dirac fermion, a vector boson or a scalar. Their masses range anywhere from a few GeV's to a few TeV's.

Astroparticle experiments are actively pursuing searches for WIMP DM candidates either directly through detection of elastic scattering of the WIMP with the nuclei in a large detector or indirectly through detection of products of DM annihilation (photons, positrons, neutrinos or antiprotons) in the Galaxy or in the Sun.

In direct detection, one measures the recoil energy deposited by the scattering of WIMPs(χ)¹ with the nuclei. Generically WIMP-nuclei interactions can be split into spin independent (scalar) and spin dependent interactions. The scalar interactions add coherently in the nucleus so heavy nuclei offer the best sensitivity. On the other hand, spin dependent interactions rely mainly on one unpaired nucleon and therefore dominate over scalar interactions only for light nuclei unless scalar interactions are themselves suppressed. In both cases, the cross-section for the WIMP nuclei interaction is typically low, so large detectors are required. Many experiments involving a variety of nuclei have been set up or are being planned. Detectors made of heavy nuclei (for example Germanium or Xenon) currently in operation include Edelweiss [15], DAMA [16], CDMS [17],

¹Here we use χ to designate the DM candidate whether a fermion, scalar or vector boson.

Xenon [18], Zeplin [20], Warp [21] and KIMS [22]. Upgrades and new projects such as Genius, Xmass [23], CLEAN [24], ArDM [25] and Eureka [26] have been proposed as well. Detectors made of light nuclei which are sensitive mainly to the spin dependent interaction include Simple [27], Picasso [28], Tokyo/NaF [29] and NAIAD [30]. The latter having one light (Na) and one heavy (I) target nuclei is actually sensitive to both spin-dependent(SD) and spin-independent(SI) interactions. Larger versions of existing detectors and new projects are also proposed, for example those operating with ^3He [32, 33]. Note that heavy nuclei although best for probing the scalar interaction have also a sensitivity to spin dependent interactions because of their odd- A isotopes. Currently the sensitivity of both types of detectors for spin dependent interactions is similar. Furthermore, different nuclei offer a sensitivity to spin dependent interactions on protons (for odd-proton nuclei such as ^{23}Na , ^{127}I or ^{19}F) or neutrons (for odd-neutron nuclei such as ^{29}Si , ^{73}Ge , ^{129}Xe).

Only one experiment, DAMA, has reported a positive signal consistent with an annihilation cross-section $\sigma_{\chi n} \approx 0.2 - 1. \times 10^{-5}$ pb for a WIMP mass around 30-100 GeV [34]. Other experiments, such as Edelweiss, CDMS, or Xenon have only set an upper limit on the WIMP-nucleon annihilation cross-section². The best limits were reported recently by Xenon, $\sigma_{\chi p}^{SI} \approx 4 \times 10^{-8}$ pb for a WIMP mass around 30 GeV [18] and by CDMS, $\sigma_{\chi p}^{SI} \approx 4.6 \times 10^{-8}$ pb for a WIMP mass around 60 GeV [19]. These values already probe a fraction of the parameter space of the most popular CDM candidate, the constrained minimal supersymmetric standard model (CMSSM) [36, 37] or some of its extensions [11] and poses severe constraints on a model with a Dirac right-handed neutrino [38]. The search for WIMPs will continue with larger detectors (around 100kg) planning to reach a level of $\sigma_{\chi n}^{SI} \approx 10^{-9}$ pb by 2010. By 2015, improved large detectors, around 1 ton, should go below the 10^{-10} pb level, for example Warp, Xenon, Eureka [26] or SuperCDMS [39]. For spin dependent interactions, the limits for neutrons from Zeplin [41] and CDMS [42] have recently been superseded by Xenon [40], $\sigma_n^{SD} \approx 5. \times 10^{-3}$ pb, while for protons the best limit from direct detection experiments was set by KIMS, $\sigma_p^{SD} \approx 0.18\text{pb}$ [31]. Indirect detection experiments looking for an excess of muon neutrinos from WIMP annihilations such as Super-Kamiokande have also set a stringent limit on the WIMP proton cross section, $\sigma_n^{SD} \approx 3. \times 10^{-3}$ pb [43]. These limits are at the level or below the positive signal reported by DAMA [34].

The calculation of the cross-section for WIMP scattering on a nucleon have been obtained at tree-level for different DM candidates: neutralinos in supersymmetry(for reviews see [44],[45]), gauge bosons in UED models [8] or in little Higgs models [46], right-handed neutrinos [47] or scalars [13, 48, 49]. Implications of the direct detection experiments on DM models have been explored for quite some time [50, 51, 52, 53, 54, 55, 56]. In the MSSM, the most complete calculation of the neutralino nucleon scattering is the one of Drees and Nojiri [57] that includes higher-order effects from twist-2 operators. Public codes for DM in the MSSM such as DarkSUSY [58] and Isajet [50] both follow this approach for calculating neutralino nucleon scattering. On the other hand, `micrOMEGAs 2.2`, a code primarily designed for the calculation of DM relic abundance did not, up to now, provide a module for the computation of the direct detection rate even though an improved tree-level computation within the MSSM has been performed for some time [59]. This is the gap we intend to fill. Here we describe the implementation of the direct DM

²Possibilities for reconciling DAMA results with other experiments have been considered in Ref. [35]

detection rate within `micrOMEGAs 2.2`.

Many ingredients enter the calculation of the direct detection rate and cover both astroparticle, particle and nuclear physics aspects. We need to know the WIMP density and the velocity distribution near the Earth. Since the WIMPs have small velocities, it means that the momentum transfer, Q^2 , is very small as compared to the masses of the WIMP and/or nuclei. The detection rate depends of course on the WIMP nucleus cross section. To arrive at the χ -nucleus cross section one has to first compute the interaction at the more fundamental level, that is at the quark level. The different matrix elements for χq interactions that capture the dynamics of the model in a perturbative way have to be converted into effective couplings of WIMPs to protons and nucleons. Finally we have to sum the proton and neutron contribution and turn this into a cross section at the nuclear level. The recoil spectrum of the nuclei depends on the velocity distribution and, in view of the low Q^2 , is contained in the elastic form factor of the nucleus. In this manual, we describe all these steps. Even though many of these steps are not new, it is necessary to understand how all the pieces are implemented in the code.

An important point to emphasize is that `micrOMEGAs`, contrary to other public codes, is not restricted to the supersymmetric model with a neutralino DM but is applicable to a generic model of new physics for DM ³. We have already in previous versions set up the code so that any model can be implemented to give the relic density of DM, the indirect detection rate and cross-sections relevant for collider applications. In the same spirit, the calculation of direct DM detection rate in nuclei is also performed for generic models of DM. More precisely the tree-level cross-section is computed in any model and dominant QCD corrections are taken into account. Other higher order corrections such as the threshold corrections to Higgs quark vertices are model dependent and are provided only for the MSSM and its extensions (CPVMSSM, NMSSM). The steps that go from the automatic computation of the cross-section for WIMP scattering on quarks to a detection rate in a large detector follow standard approaches [44]. In the spirit of the modular approach of `micrOMEGAs`, different nuclear form factors or WIMPs velocity distribution can easily be implemented by the user.

The paper is organised as follows, we first review the computation of the scattering rate for DM on a point-like nucleus starting from an effective Lagrangian for nucleon-WIMP interactions. We then show in Section 3 how to relate these to the quark-WIMP interactions and describe the method used to reconstruct the effective Lagrangian for both scalar and spin dependent interactions. We also describe the treatment of dominant QCD corrections. The computation of the recoil distribution for WIMPs scattering on nuclei taking into account nuclear form factors and velocity distribution of WIMPs follows in Section 4. The functions available in this new module are described in Section 5. Section 6 is devoted to sample results and comparisons with other codes. The treatment of box diagrams is described in Appendix A and some details about nucleus spin dependent form factors are gathered in Appendix B.

³A DM code, DM++, that can also be applied to any new physics model has been developed by [46]. This code is not yet publicly available.

2 Elastic scattering of WIMPs on point-like nuclei

The standard formalism for evaluating WIMP nuclei cross sections was reviewed in [44] with special emphasis on the case of the neutralino DM. Here we first describe the calculation of DM elastic scattering on point-like nuclei taking the Majorana fermion as an example then consider different types of DM candidates. The relation with the scattering rates on quarks, computed automatically in our code will be presented in the next section.

The velocity of DM particles near the Earth should be of the same order as the orbital velocity of the Sun, $v \approx 0.001c$. Because of this small velocity, the momentum transfer is very small as compared to the masses of the WIMP and/or nuclei. For example for typical masses of WIMP, $M_\chi \approx 100$ GeV and of nuclei, $M_A \approx 100$ GeV, the maximum transfer momentum is

$$\sqrt{-Q^2} = 2v \frac{M_\chi M_A}{M_\chi + M_A} \approx 100 \text{ MeV} \approx 0.5 \text{ fm}^{-1}. \quad (1)$$

Thus all WIMP nucleon elastic cross sections can be calculated in the limit of zero momentum transfer. The cross sections for scattering on nuclei are obtained from the WIMP nucleon cross sections after folding in the nuclei form factors, these form factors depend on the momentum transfer.

2.1 Scattering rate on point-like nuclei- the case of a Majorana fermion

In the non-relativistic limit, WIMP-nucleon elastic amplitudes can be divided into two classes, the scalar or spin independent interaction and the axial-vector or spin dependent interaction. For a spin 1/2 nucleon, interactions corresponding to multipole will clearly vanish in the zero momentum limit. In the familiar case of a Majorana fermion, the effective Lagrangian reads [60]

$$\begin{aligned} \mathcal{L}_F = & \lambda_N \bar{\psi}_\chi \psi_\chi \bar{\psi}_N \psi_N + i\kappa_1 \bar{\psi}_\chi \psi_\chi \bar{\psi}_N \gamma_5 \psi_N + i\kappa_2 \bar{\psi}_\chi \gamma_5 \psi_\chi \bar{\psi}_N \psi_N + \kappa_3 \bar{\psi}_\chi \gamma_5 \psi_\chi \bar{\psi}_N \gamma_5 \psi_N \\ & + \kappa_4 \bar{\psi}_\chi \gamma_\mu \gamma_5 \psi_\chi \bar{\psi}_N \gamma^\mu \psi_N + \xi_N \bar{\psi}_\chi \gamma_\mu \gamma_5 \psi_\chi \bar{\psi}_N \gamma^\mu \gamma_5 \psi_N \end{aligned} \quad (2)$$

In the zero momentum transfer limit the operator $\bar{\psi} \gamma_5 \psi$ vanishes while only the space component of $\bar{\psi} \gamma_5 \gamma_\mu \psi$ and the time component of $\bar{\psi} \gamma_\mu \psi$ remain. Thus the operators κ_i are suppressed in the limit of small momentum transfer by factors of order q^2/m_N^2 and/or q^2/m_χ^2 where $q^2 = -Q^2$. We will ignore these operators. Therefore only one operator survives in each class, λ_N for SI and ξ_N for SD. Of course in a specific model it is possible that the coefficient λ_N is much smaller than one of the coefficients κ_i , in which case the operator κ_i may contribute at the same level as λ_N despite the Q^2 suppression. However in this case we expect very small rates, much below the experimental sensitivities.

Spin independent interactions

For *SI* interactions with nucleons the effective Lagrangian thus reads

$$\mathcal{L}^{SI} = \lambda_N \bar{\psi}_\chi \psi_\chi \bar{\psi}_N \psi_N \quad (3)$$

where $N = p, n$. The squared amplitude for a nucleon after averaging (summing) over the polarization of incoming (outgoing) particles is,

$$|A_N^{SI}|^2 = 64 (\lambda_N M_\chi M_N)^2 \quad (4)$$

where M_N is the nucleon mass. Scalar and vector WIMP-nucleon interactions naturally induce scalar and vector WIMP-nuclei interactions. Summing on proton and neutron amplitudes gives for WIMP-nucleus interaction at rest,

$$|A_A^{SI}|^2 = 64 M_\chi^2 M_A^2 (\lambda_p Z + \lambda_n (A - Z))^2 \quad (5)$$

where Z is the nucleus charge and A the total number of nucleons. It leads to the cross section for a WIMP scattering at rest from a point-like nucleus

$$\sigma_0^{SI} = \frac{4\mu_\chi^2}{\pi} (\lambda_p Z + \lambda_n (A - Z))^2 \quad (6)$$

where μ_χ is the WIMP-nucleus reduced mass, $\mu_\chi = M_\chi M_A / (M_\chi + M_A)$. Note that the nucleon cross-section adds coherently so that there is a strong enhancement for large nuclei, $\propto A^2$ when $\lambda_p \approx \lambda_n$.

Spin dependent interactions

The effective Lagrangian for spin dependent interactions of a Majorana fermion at zero momentum transfer reads

$$\mathcal{L}^{SD} = \xi_N \bar{\psi}_\chi \gamma_5 \gamma_\mu \psi_\chi \bar{\psi}_N \gamma_5 \gamma^\mu \psi_N \quad (7)$$

It leads to the squared amplitude

$$|A_N^{SD}|^2 = 192 (\xi_N M_\chi M_N)^2 \quad (8)$$

In order to get the amplitudes for nuclei we have to sum the spin currents produced by the protons and neutrons separately. Since we know that the spins of protons with the same orbital state should be opposite, we expect strong compensation of currents produced by protons as well as those produced by neutrons. First note that for interactions at rest, the γ_0 component of the pseudovector current, Eq. 7, vanishes. The resulting interaction $\bar{\psi} \gamma_5 \gamma_i \psi$ leads to a three dimensional vector current. This vector current has to be proportional to the angular momentum J . We can write for nuclei

$$\vec{J}_N^A = S_N^A \vec{J}_A / |J_A| \quad (9)$$

where S_N^A are the expectation value of the spin content of the nucleon N in a nucleus with A nucleons. By definition, for protons and neutrons $S_p^p = S_n^n = 0.5$ and $S_p^n = S_n^p = 0$.

The second peculiarity of the SD case is a non-trivial summation over spins. Because the matrix element is proportional to \vec{J}_A the summation over spin states in a nucleus gives a factor

$$\begin{aligned} & \sum_{s_\chi, s'_\chi} \sum_{s_A, s'_A} \sum_{1 \leq k, l \leq 3} \langle s_\chi | J_\chi^k | s'_\chi \rangle \langle s'_\chi | J_\chi^l | s_\chi \rangle \langle s_A | J_A^k | s'_A \rangle \langle s'_A | J_A^l | s_A \rangle \\ &= \sum_{1 \leq k, l \leq 3} \text{tr}(J_\chi^k J_\chi^l) \text{tr}(J_A^k J_A^l) = (2J_\chi + 1) J_\chi (J_\chi + 1) (2J_A + 1) J_A (J_A + 1) / 3 \end{aligned} \quad (10)$$

here we use s, s' for labelling polarization states and J_A refers to the angular momentum of a nucleus with A nucleons. After averaging over initial polarizations, a factor $(2J_\chi + 1)(2J_A + 1)$ will cancel out.

Taking into account the spin currents structure (9) and the J dependence (10) we can write the WIMP-nucleus squared amplitudes as

$$|A^{SD}|^2 = 256 \frac{J_A + 1}{J_A} (\xi_p S_p^A + \xi_n S_n^A)^2 M_\chi^2 M_A^2 \quad (11)$$

This reduces to Eq. 8 in the special case of the nucleon and leads to the cross section at rest for a point-like nucleus [44],

$$\sigma_0^{SD} = \frac{16\mu_\chi^2}{\pi} \frac{J_A + 1}{J_A} (\xi_p S_p^A + \xi_n S_n^A)^2 \quad (12)$$

The quantities S_N^A are obtained from nuclear calculations or from simple nuclear models, such as the odd-group model. They are estimated to be ≈ 0.5 for a nuclei with an odd number of protons or neutrons and ≈ 0 for an even number. Thus no strong enhancement is expected for SD interactions in nuclei. The treatment of the nuclei form factors taking into account the momentum dependence will be discussed in section 5.2.

2.2 Generalization to other DM candidates

To derive the formulae for elastic scattering on point-like nuclei, we started from the effective WIMP-nucleon Lagrangian (3,7) written for a Majorana WIMP. In fact these can be generalized to all types of WIMPs. Our aim is to give the generic form of the effective Lagrangians for a fermionic, scalar and vectorial WIMP including the possibility of complex fields. In all cases we define the effective Lagrangian such that the normalization conditions (4,8) are satisfied. Here we write only operators that contribute at $q^2 = 0$. As we have argued for Majorana fermions, other operators are suppressed by $q^2/m_{\chi(A)}^2$ and can potentially be of the same order as the operators we consider only when both contributions to the scattering cross section are small. Note that in the case of a complex field, χ and $\bar{\chi}$ have in general different cross-sections. For each type of interaction, SI (SD) one can then construct two operators, one that is even with respect to $\chi - \bar{\chi}$ interchange, $\lambda_{N,e}(\xi_{N,e})$ and is the only remaining operator for Majorana's and another that is odd, $\lambda_{N,o}(\xi_{N,o})$.

For a fermion field the most general Lagrangian reads

$$\begin{aligned} \mathcal{L}_F &= \lambda_{N,e} \bar{\psi}_\chi \psi_\chi \bar{\psi}_N \psi_N + \lambda_{N,o} \bar{\psi}_\chi \gamma_\mu \psi_\chi \bar{\psi}_N \gamma^\mu \psi_N \\ &+ \xi_{N,e} \bar{\psi}_\chi \gamma_5 \gamma_\mu \psi_\chi \bar{\psi}_N \gamma^\mu \psi_N - \frac{1}{2} \xi_{N,o} \bar{\psi}_\chi \sigma_{\mu\nu} \psi_\chi \bar{\psi}_N \sigma^{\mu\nu} \psi_N \end{aligned} \quad (13)$$

This Lagrangian leads to matrix elements which satisfy the normalization conditions Eq. 4(8) with

$$\lambda_N = \frac{\lambda_{N,e} \pm \lambda_{N,o}}{2} \quad \text{and} \quad \xi_N = \frac{\xi_{N,e} \pm \xi_{N,o}}{2} \quad (14)$$

where the $+(-)$ signs correspond to WIMP (anti-WIMP) interactions. The special case of a self-conjugated WIMP such as the Majorana fermion is recovered when $\lambda_{N,o} = \xi_{N,o} \rightarrow 0$

and $\lambda_N = \lambda_{N_e}$, $\xi_N = \xi_{N_e}$. Note the factor 2 difference between the operator for Majorana and Dirac fermion field, compare Eq. 3 and Eq. 13. Note that the antisymmetric tensor $\sigma_{\mu\nu}$ current effectively reduces to a vector interaction since in the non-relativistic limit only the spatial components contribute.

For a scalar field only SI interactions are possible, for the general case of a complex scalar,

$$\mathcal{L}_S = 2\lambda_{N,e}M_\chi\phi_\chi\phi_\chi^*\bar{\psi}_N\psi_N + i\lambda_{N,o}(\partial_\mu\phi_\chi\phi_\chi^* - \phi_\chi\partial_\mu\phi_\chi^*)\bar{\psi}_N\gamma_\mu\psi_N \quad (15)$$

The squared amplitude is normalized as for Majorana fermions, (4), with the condition (14) for complex scalars. Again the case of the real scalar corresponds to $\lambda_{N,o} = 0$ and $\lambda_N = \lambda_{N_e}$. Note that the four-dimensional vector current $\bar{\psi}_N\gamma_\mu\psi_N$ actually leads to a scalar interaction because only the zeroth component of this current does not vanish in the non-relativistic limit.

Finally for a complex vector field,

$$\begin{aligned} \mathcal{L}_V &= 2\lambda_{N,e}M_\chi A_{\chi\mu}A_\chi^\mu\bar{\psi}_N\psi_N + \lambda_{N,o}i(A_\chi^{*\alpha}\partial_\mu A_{\chi,\alpha} - A_\chi^\alpha\partial_\mu A_{\chi\alpha}^*)\bar{\psi}_N\gamma_\mu\psi_N \\ &+ \sqrt{6}\xi_{N,e}(\partial_\alpha A_{\chi\beta}^*A_{\chi\gamma} - A_{\chi\beta}^*\partial_\alpha A_{\chi\gamma})\epsilon^{\alpha\beta\gamma\mu}\bar{\psi}_N\gamma_5\gamma_\mu\psi_N \\ &+ i\frac{\sqrt{3}}{2}\xi_{N,o}(A_{\chi\mu}A_{\chi\nu}^* - A_{\chi\mu}^*A_{\chi\nu})\bar{\psi}_N\sigma^{\mu\nu}\psi_N \end{aligned} \quad (16)$$

with in the special case of a real vector field $\lambda_{N,o} = \xi_{N,o} = 0$. Again the couplings are normalized as for the fermion case both for real (4, 8) and complex fields (14).

In `micrOMEGAs 2.2` we assume that DM particles and anti-particles have the same density. We do not consider the case where this symmetry is broken by CP violation. Under this assumption, the event rate for WIMP scattering in a large detector is obtained after averaging over χ - and $\bar{\chi}$ -nucleus cross-sections.

3 WIMP elastic scattering on quarks

The matrix elements for WIMP nucleon interactions are related to the more fundamental matrix elements for WIMP quarks interactions. These matrix elements can be easily written in a given model. To handle a generic model we rather expand WIMP quark interactions over a set of basic point-like operators. Only a few operators are necessary in the $q^2 \rightarrow 0$ limit.

The operators that are non-zero in the non-relativistic limit are similar to the operators introduced for nucleons in Eq. 13,15,16 with $\psi_N \rightarrow \psi_q$. Those operators are listed in Table 1 for either spin-independent or spin-dependent interactions of a scalar (ϕ_χ) fermion (Ψ_χ) or vector (A_χ^μ) WIMP. Note that for the latter we use the unitary gauge. Of course a scalar WIMP can only contribute to spin independent interactions. As for nucleons, the operators are separated in two classes - odd and even, depending on the symmetry properties with respect to quark - anti-quark exchange. For real WIMPs, odd operators are zero by definition.

The operators in Tables 1 have the same normalization as the operators for WIMP nucleon interactions, that is the squared matrix element for $q\chi \rightarrow q\chi$ SI interactions after summing/averaging over polarizations of outgoing/incoming particles are

$$|A_q^{SI}|^2 = 64 \left(\frac{(\lambda_{q,e} + \lambda_{q,o})}{2} M_\chi m_q \right)^2 \quad (17)$$

Table 1: Operators for WIMP - quark interactions.

	WIMP Spin	Even operators	Odd operators
SI	0	$2M_\chi \phi_\chi \phi_\chi^* \bar{\psi}_q \psi_q$	$i(\partial_\mu \phi_\chi \phi_\chi^* - \phi_\chi \partial_\mu \phi_\chi^*) \bar{\psi}_q \gamma^\mu \psi_q$
	1/2	$\bar{\psi}_\chi \psi_\chi \bar{\psi}_q \psi_q$	$\bar{\psi}_\chi \gamma_\mu \psi_\chi \bar{\psi}_q \gamma^\mu \psi_q$
	1	$2M_\chi A_{\chi\mu}^* A_\chi^\mu \bar{\psi}_q \psi_q$	$+i\lambda_{q,o}(A_\chi^{\alpha\mu} \partial_\mu A_{\chi,\alpha} - A_\chi^\alpha \partial_\mu A_{\chi\alpha}^*) \bar{\psi}_q \gamma_\mu \psi_q$
SD	1/2	$\bar{\psi}_\chi \gamma_\mu \gamma_5 \psi_\chi \bar{\psi}_q \gamma_\mu \gamma_5 \psi_q$	$-\frac{1}{2} \bar{\psi}_\chi \sigma_{\mu\nu} \psi_\chi \bar{\psi}_q \sigma^{\mu\nu} \psi_q$
	1	$\sqrt{6}(\partial_\alpha A_{\chi\beta}^* A_{\chi\nu} - A_{\chi\beta}^* \partial_\alpha A_{\chi\nu})$ $\epsilon^{\alpha\beta\nu\mu} \bar{\psi}_q \gamma_5 \gamma_\mu \psi_q$	$i\frac{\sqrt{3}}{2}(A_{\chi\mu} A_{\chi\nu}^* - A_{\chi\mu}^* A_{\chi\nu}) \bar{\psi}_q \sigma^{\mu\nu} \psi_q$

where $\lambda_{q,e}(\lambda_{q,o})$ are the coefficients of the even (odd) operators in Table 1. In the special case of a pure neutral WIMP, $(\lambda_{q,e} + \lambda_{q,o})/2 \rightarrow \lambda_q$. Similarly for SD interactions the normalization is specified in Eq. 8.

3.1 Numerical approach to operator expansion

The `micrOMEGAs 2.2` package contains an automatic generator of matrix elements, CalcHEP [76]. For each model, `micrOMEGAs` has a complete list of Feynman rules which specify the model in the CalcHEP format. Therefore CalcHEP can generate automatically amplitudes for $\chi q \rightarrow \chi q$ for any kinematics. Here we need to generate these matrix elements at low energy in a format that can be easily and automatically turned into effective operators for χ -nucleon interactions. So we want to expand automatically the Lagrangian of the model in terms of local operators and extract the coefficients of the low energy effective WIMP quark Lagrangian

$$\hat{\mathcal{L}}_{eff}(x) = \sum_{q,s} \lambda_{q,s} \hat{\mathcal{O}}_{q,s}(x) + \xi_{q,s} \hat{\mathcal{O}}'_{q,s}(x) \quad (18)$$

where q is a label for quark, s is a label for even and odd operators and $\hat{\mathcal{O}}_{q,s}$ ($\hat{\mathcal{O}}'_{q,s}$) are the spin independent (dependent) operators in Table 1. Traditionally the coefficients $\lambda_{q,s}, \xi_{q,s}$ are evaluated symbolically using Fiertz identities in the limit $q^2 \ll M_A^2$. Instead in `micrOMEGAs 2.2` these coefficients are estimated numerically using projection operators. First we compute special matrix elements for $\chi q \rightarrow \chi q$ scattering at zero momentum transfer. For this we need to add to the model Lagrangian the projection operators defined in Table 1. The interference between one projection operator and the effective vertices will single out either the spin dependent or spin independent contribution, since the effective Lagrangian is written in an orthogonal basis. To further separate the coefficient of the even and odd operators, we compute both $\chi q \rightarrow \chi q$ and $\chi \bar{q} \rightarrow \chi \bar{q}$ matrix elements. We use the fact that for a given projection operator the interference term in the squared matrix elements for quarks are identical to those for antiquarks for even operators and

have opposite signs for odd operators. Thus, taking into account the normalisation,

$$\begin{aligned}\lambda_{q,e} + \lambda_{q,o} &= \frac{-i\langle q(p_1), \chi(p_2) | \hat{S} \hat{\mathcal{O}}_{q,e} | q(p_1), \chi(p_2) \rangle}{\langle q(p_1), \chi(p_2) | \hat{\mathcal{O}}_{q,e} \hat{\mathcal{O}}_{q,e} | q(p_1), \chi(p_2) \rangle} \\ \lambda_{q,e} - \lambda_{q,o} &= \frac{-i\langle \bar{q}(p_1), \chi(p_2) | \hat{S} \mathcal{O}_{q,e} | \bar{q}(p_1), \chi(p_2) \rangle}{\langle \bar{q}(p_1), \chi(p_2) | \hat{\mathcal{O}}_{q,e} \hat{\mathcal{O}}_{q,e} | \bar{q}(p_1), \chi(p_2) \rangle}\end{aligned}\tag{19}$$

where the S -matrix, $\hat{S} = 1 - i\mathcal{L}$ is obtained from the complete Lagrangian at the quark level.

To implement this procedure, a new model file is created automatically in `micrOMEGAs 2.2`. This file contains the model file of a given model as well as the auxiliary vertices of Table 1. There is no need for the user to implement these auxiliary vertices. CalcHEP then generates and calculates symbolically all diagrams for WIMP - quark/anti-quark elastic scattering keeping only the squared diagrams which contains one normal vertex and one auxiliary vertex. This corresponds to the matrix elements in Eq. 19. Note that in the file that defines the model all quarks should be defined as massive particles. Vertices that depend on light quark masses cannot be neglected, for example the couplings of Higgs to light quarks, since the dominant term for WIMP quark scalar interactions is proportional to quark masses. In particular in SUSY models masses of the first and second generation fermions must be included. When converting to WIMP nucleon interactions this quark mass will get replaced by a nucleon mass so that the nucleon cross section is independent of the light quark masses, see Section 3.3. Because the amplitude for WIMP scattering on light quarks is proportional to a small quark masses, one has to be wary of numerical instabilities. To avoid these we consider the amplitude for $q(p_1)\chi(p_2) \rightarrow q(p_3)\chi(p_4)$ and write the squared matrix element in terms of the dot products $p_1.p_2$ and $p_1.p_3$. The amplitude depends explicitly on the small momenta p_1 thus avoiding the numerical instabilities in matrix elements that were found with other kinematics.

3.2 Contribution of tensor (twist-2) operators.

There are other point-like operators which produce the same SI and SD amplitudes at zero momentum. They are the operators containing field derivatives. Here we consider the contributions of the symmetric traceless tensor operator to the WIMP nucleon scattering. A complete treatment of twist-2 operators in neutralino nucleon elastic scattering in the MSSM was first presented in [57]. In the MSSM tensor operators come from the momentum expansion of the denominator in the squark exchange diagram and are usually suppressed by a factor $M_N/(M_{\bar{q}} - M_\chi)$ with respect to the main contribution. Thus they are expected to be mainly relevant when the squark is not much heavier than the WIMP, for example in the coannihilation region.

In the MSSM, the tensor operator reads [57],

$$\mathcal{O}_{q,t} = \frac{1}{2}(\bar{\chi}\gamma_\mu\partial_\nu\chi)\mathcal{O}_q^{\mu\nu}\tag{20}$$

$$\mathcal{O}_q^{\mu\nu} = \bar{q}(\gamma^\mu\overrightarrow{\partial}^\nu - \gamma^\mu\overleftarrow{\partial}^\nu + \gamma^\nu\overrightarrow{\partial}^\mu - \gamma^\nu\overleftarrow{\partial}^\mu + im_qg^{\mu\nu})q\tag{21}$$

where $\mathcal{O}_q^{\mu\nu}$ is a twist-2 operator (recall that *twist* is defined as *dimension - spin*). Note that this tensor operator is generically found in other models where new coloured particles couple to WIMP and quarks.

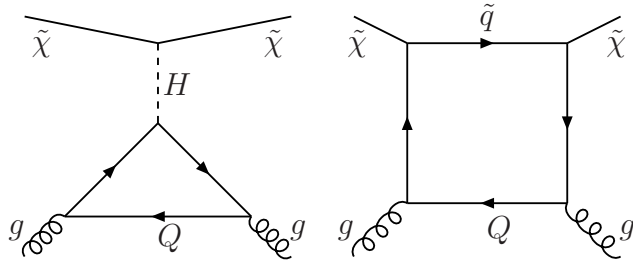


Figure 1: Diagrams that contribute to WIMP-gluon interaction via quark loops in the MSSM.

To extract automatically the coefficient of the tensor operator in the low energy WIMP quark Lagrangian we consider forward scattering at small momentum. Indeed for such kinematics the matrix element of the product of two scalar operators does not depend on the collision while the product of scalar and tensor does since

$$\langle q(p_1), \chi(p_2) | \mathcal{O}_{q,t} \mathcal{O}_{q,e} | q(p_1), \chi(p_2) \rangle = -32m_q M_\chi (4(p_1 \cdot p_2)^2 - m_q^2 M_\chi^2) \quad (22)$$

Thus the tensor operator can be extracted by evaluating numerically the second derivative of

$$\langle q(p_1), \chi(p_2) | \hat{S} \mathcal{O}_{q,e} | q(p_1), \chi(p_2) \rangle \quad (23)$$

with respect to $p_1 \cdot p_2$. Note that this trick does not require that one implements the tensor operators in the `CalcHEP` model. Since the tensor operators contribute also to the amplitude at rest, after extracting the coefficient of the tensor operator it should be subtracted from Eq. 19 to isolate the coefficient of the scalar operator.

In typical MSSM models the correction due to an accurate treatment of twist-2 operators is less than 1%, in special cases though, for example for a small mass difference between the squark and the WIMP the contribution can be larger. The contribution of higher spin twist-2 operators are in general further suppressed and are not included here. In the MSSM we have compared numerically the cross sections obtained with our method for extracting the effective operators, including the twist-2 operators, with the complete results of Drees and Nojiri [57]. For this we have implemented their analytical results, correcting a sign in the SD amplitude between Z and squark exchange. We found numerical agreement at the percent level.

3.3 Nucleon form factors

In order to convert WIMP-quark amplitudes to WIMP-nucleon amplitudes, we need to know the values of the quark currents inside the nucleon. The operators for these quark currents in a nucleon can be extracted from experiment or estimated theoretically. In the following we give estimates for the coefficients of the four quark currents listed in Table 1

3.3.1 Scalar coefficients

The scalar $\bar{\psi}_q \psi_q$ current characteristic of the SI-even interaction depends on the total number of quarks and anti-quarks in the nucleon. The operator $\langle N | m_q \bar{\psi}_q \psi_q | N \rangle$ is interpreted

as the contribution of quark q to the nucleon mass, M_N ,

$$\langle N | m_q \bar{\psi}_q \psi_q | N \rangle = f_q^N M_N \quad (24)$$

where the coefficients f_q^N relate nucleon and quark operators,

$$\lambda_{N,p} = \sum_{q=1,6} f_q^N \lambda_{q,p} \quad (25)$$

Note there is no explicit dependence on the quark mass in the cross section for WIMP nucleon scattering. Indeed the quark mass term gets transformed into a nucleon mass. For heavy quarks, Q , the parameter f_Q^N is induced via gluon exchange with the nucleon, see section 3.5, and [77]

$$f_Q^N = \frac{2}{27} \left(1 - \sum_{q \leq 3} f_q^N \right) \quad (26)$$

The coefficients f_q^N can be determined using the value of the light quark masses extracted from baryon masses, the ratio of the quantities $B_q = \langle N | \bar{q}q | N \rangle$ for u, d and s quarks and from the value of the pion-nucleon sigma-term. It is the latter that has the largest uncertainty, see for example [79, 80]. For light quark masses ratio we take

$$\frac{m_u}{m_d} = 0.553 \pm 0.043, \quad \frac{m_s}{m_d} = 18.9 \pm 0.8 \quad (27)$$

We define the quantities

$$z = \frac{B_u - B_s}{B_d - B_s} \approx 1.49 \quad \text{and} \quad y = \frac{2B_s}{B_u + B_d} \quad (28)$$

where y denotes the fractional strange quark content of the nucleon. y is obtained from the pion-nucleon sigma term and the quantity σ_0 which is related to the size of the SU(3) symmetry breaking effect [81]

$$\sigma_{\pi N} = \frac{(m_u + m_d)}{2} (B_u + B_d); \quad \sigma_0 = \frac{m_u + m_d}{2} (B_u + B_d - 2B_s) \quad (29)$$

which implies

$$y = 1 - \frac{\sigma_0}{\sigma_{\pi N}}. \quad (30)$$

Recent analyses suggest that [82]

$$\sigma_{\pi N} = 55 - 73 \text{ MeV} \quad \text{and} \quad \sigma_0 = 35 \pm 5 \text{ MeV} \quad (31)$$

where σ_0 is estimated from chiral perturbation theory [81] or from baryon mass differences [83]. Defining

$$\alpha = \frac{B_u}{B_d} = \frac{2z - (z - 1)y}{2 + (z - 1)y} \quad (32)$$

the parameters for light quarks in the proton write

$$f_d^p = \frac{2\sigma_{\pi N}}{\left(1 + \frac{m_u}{m_d}\right)m_p(1 + \alpha)}, \quad f_u^p = \frac{m_u}{m_d} \alpha f_d^p, \quad f_s^p = \frac{\sigma_{\pi N} y}{\left(1 + \frac{m_u}{m_d}\right)m_p} \frac{m_s}{m_d} \quad (33)$$

and in the neutron

$$f_d^n = \frac{2\sigma_{\pi N}}{(1 + \frac{m_u}{m_d})m_n} \frac{\alpha}{(1 + \alpha)}, \quad f_u^n = \frac{m_u}{m_d} \frac{1}{\alpha} f_d^n, \quad f_s^n = \frac{\sigma_{\pi N} y}{(1 + \frac{m_u}{m_d})m_n} \frac{m_s}{m_d} \quad (34)$$

As default values we take $\sigma_0 = 35$ MeV and $\sigma_{\pi N} = 55$ MeV which lead to

$$\begin{aligned} f_d^p &= 0.033, & f_u^p &= 0.023, & f_s^p &= 0.26 \\ f_d^n &= 0.042, & f_u^n &= 0.018, & f_s^n &= 0.26 \end{aligned} \quad (35)$$

In `micrOMEGAs 2.2`, the values for these coefficients can be changed directly or through modification of σ_0 and $\sigma_{\pi N}$ and the quark mass ratios. In all cases the parameters for heavy quarks will be recalculated using Eq. 26. Note that f_s^N is typically larger than the value used in earlier analyses, $f_s^p = 0.118 - 0.14$. This is mainly due to an increase in $\sigma_{\pi N}$ which was centered around 45 MeV [84, 85]. This large correction to f_s^N can lead to an increase by a factor 2-6 in the spin independent cross-section for nucleons [51]. Furthermore even with the new estimate of $\sigma_{\pi N}$, large uncertainties remain.

3.3.2 Vector coefficients

The vector $\bar{\psi}_q \gamma_\mu \psi_q$ current in the SI-odd interaction is responsible for the difference between χN and $\bar{\chi} N$ cross sections. The interpretation of this current is very simple. It counts the number of quarks minus the number of anti-quarks in the nucleon, that is the number of valence quarks. This current is the only one that does not suffer from theoretical uncertainties when going from the WIMP- quark interaction to the WIMP-nucleon interaction. Indeed only valence quarks contribute to the vector current so that

$$\lambda_{N,o} = \sum_{q=u,d} f_{V_q}^N \lambda_{q,o} \quad (36)$$

with $f_{V_u}^p = 2, f_{V_d}^p = 1, f_{V_u}^n = 1, f_{V_d}^n = 2$.

3.3.3 Axial-vector coefficients

The axial-vector current $\bar{\psi}_q \gamma_\mu \gamma_5 \psi_q$ is responsible for spin dependent interactions. It counts the total spin of quarks and anti-quarks q in the nucleon. Operators for axial-vector interactions in the nucleon are related to those involving quarks,

$$\xi_{N,e} = \sum_{q=u,d,s} \Delta q^N \xi_{q,e} \quad (37)$$

with

$$2s_\mu \Delta q^N = \langle N | \bar{\psi}_q \gamma_\mu \gamma_5 \psi_q | N \rangle \quad (38)$$

Here s_μ is the nucleon spin and Δq^N are extracted from lepton-proton scattering data. The strange contribution to the spin of the nucleon, as measured by EMC and SMC turned out to be much larger than expected from the naive quark model [86]. This leads to the following estimates for the light quark contributions in the proton which have been used in many analyses of DM spin dependent interactions,

$$\Delta_u^p = 0.78 \pm 0.02, \quad \Delta_d^p = -0.48 \pm 0.02, \quad \Delta_s^p = -0.15 \pm 0.02 \quad (39)$$

These early results have qualitatively been confirmed by HERMES [87] and also by COMPASS [88]. As default values for the axial-vector coefficients we use the latest determination of the light quark contributions [87],

$$\Delta_u^p = 0.842 \pm 0.012, \quad \Delta_d^p = -0.427 \pm 0.013, \quad \Delta_s^p = -0.085 \pm 0.018 \quad (40)$$

These results are obtained in the limit of $SU(3)_F$ symmetry. It is argued that flavour symmetry breaking effects might lead to an additional shift in the strange quark contribution, thus making this value compatible with the value extracted from EMC and SMC [86]. We neglect the heavy quark contribution to the proton spin since they have been shown to be small [89]. The neutron quantities are simply obtained by an isospin rotation

$$\Delta_u^n = \Delta_d^p, \quad \Delta_d^n = \Delta_u^p, \quad \Delta_s^n = \Delta_s^p \quad (41)$$

Note that because there can be a cancellation between the Δq 's when summing over light quarks in the nucleon, there can be a strong reduction in the coupling of WIMPs to neutrons or protons when varying the quark coefficients within the error bars.

3.3.4 Coefficients of the $\sigma_{\mu\nu}$ term

The tensor current, $\bar{\psi}_q \sigma_{\mu\nu} \psi_q$ in SD-odd interactions is responsible for the difference between χN and $\bar{\chi} N$ spin-dependent cross sections. This current can be interpreted as the difference between the spin of quarks and the spin of anti-quarks in nucleons. Recent measurements by COMPASS [90] and HERMES [91] indicate that the antiquark contribution ($\delta\bar{u}^N + \delta\bar{d}^N$) is compatible with zero. Forthcoming COMPASS data on muon scattering off a proton target will provide a separate determination of $\Delta\bar{u}^p$ and $\Delta\bar{d}^p$ [90]. If confirmed to be zero, it would mean that the coefficients for the tensor interaction are identical to those for the axial vector interaction. The tensor coefficients have also been computed on the lattice, for example Ref. [92] gives

$$\delta_u^p = 0.84, \quad \delta_d^p = -0.23, \quad \delta_s^p = -0.05. \quad (42)$$

These results were later confirmed by another lattice calculation of the LHPC collaboration [93]. We do not attempt to estimate the uncertainty associated with the lattice computation of the tensor coefficients. Note that both collaborations also compute the axial-vector coefficients on the lattice and they find values compatible (with larger uncertainties) to the one obtained from COMPASS and HERMES data. In our code it is possible to modify the input values for the tensor coefficients independently of the axial-vector coefficients.

3.4 Twist-2 coefficients

The nucleon form factors for twist-2 operators are well known in QCD. For the operator $\mathcal{O}_{q,t}^{\mu\nu}$, eq. 21, we have [57]

$$\langle N(p) | \mathcal{O}_{q,t}^{\mu\nu} | N(p) \rangle = (p^\mu p^\nu / M_N - g^{\mu\nu} M_N / 4) \int_0^1 (q(x) + \bar{q}(x)) x dx \quad (43)$$

where $q(x)$ and $\bar{q}(x)$ are parton distribution functions calculated at the scale $Q = M_{\bar{q}} - M_\chi$. We use the CTEQ6L distribution functions [94]. The computation of the box diagrams

for neutralino gluon scattering in [57] leads to a loop improved twist-2 tensor form factor containing gluon densities instead of quark parton densities. However these authors argued that the tree-level approach was more robust for c and b quarks because of large logs in the loop result, $\log(Q/m_q)$. In our package we use the tree level formulae for both c and b quarks and we neglect the twist-2 form factor for t quarks. ⁴

3.5 Gluon contribution and QCD corrections to the scalar amplitude

The nucleon consists of light quarks and gluons, nevertheless one can also consider interactions of WIMPs with heavy quarks inside the nucleon. These effectively come into play since heavy quark loops contribute to the interactions of WIMP with gluons, see for example the diagrams in Fig. 1. It is well known that when Higgs exchange dominates, see for example [57], WIMP gluon interactions via heavy quark loops can be taken into account by considering WIMP interactions with heavy quarks together with an estimation of the heavy quark condensates in nucleons. Furthermore dominant QCD corrections can also be taken into account in that case [95].

The anomaly of the trace of energy-momentum tensor in QCD implies [77]

$$M_N \langle N|N \rangle = \langle N| \sum_{q \leq n_f} m_q \bar{\psi}_q \psi_q (1 + \gamma) + \left(\frac{\beta^{n_f}}{2\alpha_s^2} \right) \alpha_s G_{\mu\nu} G^{\mu\nu} |N \rangle \quad (44)$$

where γ is the anomalous dimension of the quark field operator, α_s the strong coupling constant, $G_{\mu\nu}$ the gluon field tensor and $\beta^{n_f} = -\alpha_s^2/4\pi(11 - 2n_f/3 + \alpha_s/4\pi(102 - 38n_f/3))$. In the leading order approximation for three flavours, Eq.(44) is simplified to

$$M_N \langle N|N \rangle = \langle N| \sum_{q=u,d,s} m_q \bar{\psi}_q \psi_q - \frac{9}{8\pi} \alpha_s G_{\mu\nu} G^{\mu\nu} |N \rangle \quad (45)$$

Comparing Eq. 44 for n_f and $n_f + 1$ one finds the contribution of one heavy quark flavour to the nucleon mass, relating the heavy quark content of the nucleon to the gluon condensate

$$\langle N|m_Q \bar{\psi}_Q \psi_Q |N \rangle = -\frac{\Delta\beta}{2\alpha_s^2(1 + \gamma)} \langle N|\alpha_s G_{\mu\nu} G^{\mu\nu} |N \rangle \quad (46)$$

where $\Delta\beta$ is a contribution of one quark flavor to the QCD β -function. This formula agrees with the effective $HG_{\mu\nu}G^{\mu\nu}$ vertex at small q^2 [96]. Up to order α_s^2 ,

$$\langle N|m_Q \bar{\psi}_Q \psi_Q |N \rangle = -\frac{1}{12\pi} \left(1 + \frac{11\alpha_s(m_Q)}{4\pi} \right) \langle N|\alpha_s G_{\mu\nu} G^{\mu\nu} |N \rangle \quad (47)$$

Keeping only the leading order and combining with Eq. 45 will lead to the usual relation Eq. 26. Note that the NLO terms in Eq. 44 partially cancel the effect of the NLO corrections in Eq. 47 so that the QCD corrections to Eq. 26 are small. See also [97] for an alternative estimate of the heavy quark content of the nucleon.

⁴Note that we evaluate the parton distributions at a scale $Q = M_{\tilde{q}} - M_\chi$ rather than $Q = (M_{\tilde{q}}^2 - M_\chi^2)^{1/2}$ as suggested in [57]. In this case we find that the loop and tree-level approaches agree reasonably well for b -squarks when $M_{\tilde{b}} - M_\chi \approx 20$ GeV. Larger mass differences give a very small contribution from the twist-2 term while smaller mass differences typically lead to a low value for the DM relic density.

The simplest way to take into account dominant QCD corrections to Higgs exchange is then to consider WIMP heavy quark interactions through Higgs exchange and introduce an effective vertex for heavy quarks in the nucleon with Eq. 26 modified to include one-loop QCD corrections, Eq. 47. The equivalence of this approach with the description of the Higgs coupling to the nucleon through gluons is confirmed by a direct computation of the triangle diagram of Fig.1 in the limit where $Q^2 \ll M_Q$. Recall that the typical transfer momentum is $Q \approx 100$ MeV, Eq. 1. Note that for light quarks the corrections that would arise from their contribution to the triangle diagram that couples a Higgs to gluon are all absorbed into the definition of the light quark content of the nucleon.

While triangle diagrams can be treated using effective heavy quark nucleon condensate instead of performing an explicit one-loop calculation, such a simple treatment is not justified in general for box diagrams. Such an approximation would be valid only when $m_q/(M_{\tilde{q}} - M_\chi) \ll 1$ as shown explicitly in [57] for the MSSM. In that case the tree-level approach works well for c and b quarks but would fail for t-quarks unless the associated squark is much heavier. Nevertheless this is the approximation we use by default in **micrOMEGAs**, the main reason being that in many models the contribution of the Higgs exchange diagram is much larger than the one from the box diagrams. The user can always ignore this simple treatment and implement a more complete calculation of the box diagrams. For example in the case of MSSM-like we have implemented the one-loop computation of the neutralino nucleon scattering of Ref. [57], see Section 4 and Appendix A.

In a generic new physics model, new heavy coloured particles can also contribute to the WIMP gluon amplitude, for instance squarks in the MSSM. For heavy quarks, the computation of the triangle diagrams involving squarks, or any other scalar colour triplet, also reduces to a calculation of WIMP-squark scattering with an estimation of the squark content in the nucleon. The latter can be obtained by calculating the contribution of squarks to the QCD β -function just as was done for heavy quarks, Eq. 46. Note however that the contribution of scalars to the trace anomaly has an additional factor of 2 due to the different dimension of scalar and fermion fields. After substituting $\Delta\beta$ and γ we get at order α_s ,

$$\langle N | 2M_Q^2 \phi_{\tilde{Q}}^* \phi_{\tilde{Q}} | N \rangle = -\frac{1}{48\pi} \left(1 + \frac{25\alpha_s}{6\pi} \right) \langle N | \alpha_s G_{\mu\nu} G^{\mu\nu} | N \rangle \quad (48)$$

Thus the contribution of scalars is expected to be small because of small scalar content in the nucleon. This relation is also known to order α_s^2 [95]. On the other hand other new particles such as a heavy Majorana fermion or a real scalar which belong to adjoint color representation have very large nucleon densities

$$\langle N | m_Q \bar{\psi}_Q \psi_Q | N \rangle = -\frac{1}{2\pi} \langle N | \alpha_s G_{\mu\nu} G^{\mu\nu} | N \rangle \quad (49)$$

$$\langle N | 2M_Q^2 \phi_{\tilde{Q}} \phi_{\tilde{Q}} | N \rangle = -\frac{1}{8\pi} \langle N | \alpha_s G_{\mu\nu} G^{\mu\nu} | N \rangle \quad (50)$$

In summary, in **micrOMEGAs** we check the list of coloured particles in the model and according to their spin and colour define the nucleon content for each particle using Eq. 47-50. We then compute the contributions from all WIMP-coloured particles processes. The coefficients of the operators for such interactions are calculated automatically in the same manner as the coefficients for WIMP-quarks interactions as described in Section 3.1. The case of of a color octet vector particle is not treated.

4 The special case of supersymmetry

In the case of the MSSM, additional corrections to both the Higgs exchange diagram and the box diagrams with quarks or squark exchange have been computed explicitly. These corrections can easily be extended to the case of the CPVMSSM with complex phases and of the NMSSM with an extra singlet field.

The main contribution to the scalar neutralino nucleon cross section involves the Higgs exchange diagram with the Higgs coupling to light quark pairs. While in the computation of the relic density one could safely neglect the Higgs coupling to light quarks, for direct detection this approximation is no longer valid. The MSSM model file must therefore be modified accordingly. Furthermore SUSY-QCD corrections to the Higgs exchange diagrams can be large and should be taken into account. In particular the gluino-squark loops can give large corrections to all $H_i \bar{q}q$ couplings ($H_i = h, H, A$), they are also related to the corrections to the quark masses [78]. These SUSY-QCD corrections will induce couplings of the quarks to the 'wrong' Higgs doublet and are enhanced by $\tan \beta$ for down type quarks. The SUSY-QCD corrections to the $H_i \rightarrow \bar{b}b$ vertices are already taken into account in `micrOMEGAs` for the computation of the relic density of DM and are also important for the computation of $b \rightarrow s\gamma$. We generalize this to include the SUSY-QCD corrections for all down-type quarks [95]. As in `micrOMEGAs_1.3`, we define the effective Lagrangian

$$\begin{aligned} \mathcal{L}_{eff} = \sqrt{4\pi\alpha_{QED}} \frac{m_q}{1 + \Delta m_q} \frac{1}{2M_\chi \sin \theta_W} & \left[-Hq\bar{q} \frac{\cos \alpha}{\cos \beta} \left(1 + \frac{\Delta m_q \tan \alpha}{\tan \beta} \right) \right. \\ & \left. + iAq\bar{q} \tan \beta \left(1 - \frac{\Delta m_q}{\tan \beta^2} \right) + hq\bar{q} \frac{1}{\cos \beta} \left(1 - \frac{\Delta m_q}{\tan \alpha \tan \beta} \right) \right] \end{aligned} \quad (51)$$

where $q = d, s, b$. We use the same conventions as in [98] for the supersymmetric model parameters and our code is compatible with the SUSY Les Houches Accord (SLHA) [99]. For light quarks, $\Delta m_{d,s}$ includes only the squark gluino loop while additional electroweak corrections which are important for the third generation are included in Δm_b [98]. These corrections are much smaller and can be neglected for up type quarks. As we mentioned before there is no explicit dependence on the quark mass for the scalar neutralino nucleon cross section, nevertheless the effect of SUSY-QCD corrections remains.

Other vertices that contribute to neutralino quark interactions and also have a dependence on the light quark mass are the $\tilde{\chi}_1^0 \tilde{q}q$ vertices. These vertices involve a coupling of the Higgsino component which is proportional to the quark mass as well as a coupling of the gaugino component which depends on the squark mixing matrix. Since the off-diagonal element of the 2X2 mixing matrix for a given squark flavour is also proportional to the quark mass, mixing cannot be neglected even for the first two generations. The MSSM model therefore needs to be modified to add these extra terms in vertices for light quarks. In general, input parameters for `micrOMEGAs` are taken from the SLHA [99] and assume no mixing for the first two generations, we define the mixing angle as

$$\tan 2\phi_q = -2 \frac{m_q \tilde{A}_q}{M_{\tilde{q}_R}^2 - M_{\tilde{q}_L}^2} \quad (52)$$

where $\tilde{A}_u = A_u - \mu/\tan \beta$ for up-type quarks and $\tilde{A}_d = A_d - \mu \tan \beta$ for down-type quarks, m_q is the quark mass including SUSY-QCD corrections [78]. For third generation

sfermions, the mixing angle is taken directly from the spectrum calculator as given in the SLHA [99]⁵.

The importance of QCD and Δm_b corrections in a few sample supersymmetric models is displayed in Table 2. A more detailed description of the parameters of the models considered can be found in Tables 5, 7. The QCD corrections in Eqs. 47,48 are relevant only for heavy quarks and will always lead to an increase of the spin independent cross section, typically around 5%. The SUSY-QCD corrections on the other hand depend on the sign of μ and are enhanced at large values of $\tan\beta$. In the decoupling limit, these corrections affect mainly the couplings of heavy Higgses as well as the couplings of squarks while the light Higgs, which often gives the dominant contribution to the scalar cross section remains unchanged. For $\mu > 0$, $\Delta m_q > 0$ and the cross section decreases, so that the net effect of the QCD and SUSY-QCD corrections remains small. For $\mu < 0$, $\Delta m_q < 0$ and both the heavy Higgs and squark contribution increases. In the sample model KP of Table 2 the SUSY QCD corrections lead to a mild decrease of σ_n^{SI} , this is because there is a destructive interference between the dominant light Higgs exchange and the heavy Higgs and squark diagrams.

Table 2: Effect of higher-order corrections on σ_n^{SI} in sample SUSY models.

	BP	KP	IP	NUH	MSSM1
$\tan\beta$	10	40	35	30	10
μ	+	-	+	+	+
Ωh^2	0.101	0.101	0.113	0.088	0.100
$\sigma_n^{SI} \times 10^9 pb$ tree-level	8.25	8.63	26.1	9.12	19.1
QCD	8.50	9.13	26.8	9.36	19.8
Δm_b	7.53	8.52	20.0	7.75	18.1
QCD+ Δm_b	7.77	9.02	20.5	7.97	18.7
QCD+ Δm_b +box	7.78	9.02	20.5	7.97	18.7

Finally in the MSSM and its extensions we also compute more precisely one-loop corrections. In that case we replace the tree-level treatment of heavy quarks by a one-loop computation of the process $\chi g \rightarrow \chi g$ including triangle and box diagrams involving quarks and squarks. The corrections to the dominant Higgs exchange triangle diagram discussed above are always included so the bulk of the corrections are taken into account with either option. The one-loop correction from the box diagram is obtained by modifying the denominators entering the tree-level diagrams, details can be found in Appendix A. This method reproduces the complete results of Drees and Nojiri [57]. We have implemented these analytic results and provide a special routine that can be used for comparing the two approaches. In the last two lines of Table 2 we compare the results using heavy quark currents with the ones including the more complete treatment of loop corrections (box diagrams). In mSUGRA models where the Higgs exchange diagrams dominate,

⁵In the case of Isajet, we set $A_d = A_s = A_b$ and $A_u = A_c = A_t$. Note that this assumption is not strictly correct but the mixing in the down-squark sector is in any case dominated by the $\mu \tan\beta$ term while in the up-squark sector it is mostly relevant for the top squark.

discrepancies are below the per-cent level. Larger discrepancies can be found in the general MSSM, where, based on explicit calculations, we expect loop corrections to be of order $m_q/(M_{\tilde{q}} - M_\chi)$. This can be large for heavy quarks specially when squark masses are of the same order as the neutralino masses.

5 Scattering rates on nuclei: form factors and velocity distribution

To get the rate for direct detection of WIMPs as a function of the recoil energy of the nucleus we must take into account both the finite velocity of WIMPs and the nucleus form factor.

5.1 Spin independent interactions

First consider the simplest case of the SI interaction. We note that ignoring form factor effects, we expect isotropic scattering in the center of mass frame. This means that in the laboratory frame for a WIMP of velocity v one gets a constant distribution over the recoil energy in the interval $0 < E < E_{max}(v)$. In the non-relativistic approximation,

$$E_{max}(v) = 2 \left(\frac{v^2 \mu_\chi^2}{M_A} \right) \quad (53)$$

For an incoming WIMP with a fixed velocity the recoil energy distribution is thus of the form

$$\frac{d\sigma_A^{SI}}{dE} = \sigma_0^{SI} \frac{\Theta(E_{max}(v) - E) F_A^2(q)}{E_{max}(v)} \quad (54)$$

where $F_A(q)$ is the nucleus form factor which depends on the transfer momentum $q = \sqrt{2EM_A}$.

DM particles have a certain velocity distribution, $f(v)$. After integration over incoming velocities, the distribution of the number of events over the recoil energy reads

$$\frac{dN^{SI}}{dE} = \frac{2M_{det}t}{\pi} \frac{\rho_0}{M_\chi} F_A^2(q) (\lambda_p Z + \lambda_n (A - Z))^2 I(E) \quad (55)$$

where ρ_0 is the DM density near the Earth, M_{det} the mass of the detector and t the exposure time and

$$I(E) = \int_{v_{min}(E)}^{\infty} \frac{f(v)}{v} dv \quad (56)$$

$$v_{min}(E) = \left(\frac{EM_A}{2\mu_\chi^2} \right)^{1/2} \quad (57)$$

For SI interactions, the form factor is a Fourier transform of the nucleus distribution function,

$$F_A(q) = \int e^{-iqx} \rho_A(x) d^3x \quad (58)$$

where $\rho_A(x)$ is normalized such that $F_A(0) = 1$. In our package, we use the Fermi distribution function

$$\rho_A(r) = \frac{c_{norm}}{1 + \exp((r - R_A)/a)} \quad (59)$$

where c_{norm} is fixed by the normalization condition. The resulting form factor is often referred to as the Woods-Saxon form factor [44]. The parameters R_A and a can be extracted from muon scattering data. Compilations of these parameters for several nuclei are available [62, 63]. A two-parameter fit to these tables [64] gives

$$R_A = 1.23A^{\frac{1}{3}} - 0.6\text{fm} \quad (60)$$

for a surface thickness, $a = 0.52$ fm. This is the default value we use for all nuclei. We have tested this interpolation. Using the data on the first three radial moments of charge distribution [62] we calculate the form factor at a recoil energy of 15 keV, a value slightly above threshold for DM detectors. We then calculate the half-density radius R_A which reproduces this value. Fig. 2 shows that for various nuclei, the value of R_A extracted this way is well approximated by Eq. 60.

5.2 Spin dependent interactions

The *SD* case features the same kinematics as the case just discussed. The simplest approximation would be to assume that the S_N^A coefficients have the same q -dependence as the *SI* form factor (58). For a more precise evaluation of the q dependence, one should note that when $q \neq 0$ the vectors \vec{J}_p and \vec{J}_n are not collinear anymore. As a result, three form factors need to be introduced. They correspond to the three coefficient of the quadratic function of ξ_p^2, ξ_n^2 and $\xi_p \xi_n$ in the squared amplitude, Eq. 12. Equivalently, one can construct the isoscalar and isovector combinations

$$a_0 = \xi_p + \xi_n \quad (61)$$

$$a_1 = \xi_p - \xi_n \quad (62)$$

so that the SD recoil energy distribution for a fixed WIMP velocity reads

$$\frac{d\sigma_A^{SD}}{dE} = \frac{16\mu_\chi^2}{2J_A + 1} (S_{00}(q)a_0^2 + S_{01}(q)a_0a_1 + S_{11}(q)a_1^2) \frac{\Theta(E_{max}(v) - E)}{E_{max}(v)}. \quad (63)$$

The coefficients $S_{00}(q)$, $S_{11}(q)$, and $S_{01}(q)$ are the nuclear structure functions which take into account both the magnitude of the spin in the nucleon and the spatial distribution of the spin. They are normalized such that [65]

$$\begin{aligned} S_{00}(0) &= C(J_A)(S_p + S_n)^2 \\ S_{11}(0) &= C(J_A)(S_p - S_n)^2 \\ S_{01}(0) &= 2C(J_A)(S_p + S_n)(S_p - S_n) \\ \text{where } C(J_A) &= \frac{(2J_A + 1)(J_A + 1)}{4\pi J_A} \end{aligned} \quad (64)$$

With this normalization, one recovers the cross section at rest, Eq. 12, starting from Eq. 63.

After taking into account the velocity distribution, the distribution for the number of events over the nuclei recoil energy for spin dependent interactions reads

$$\frac{dN^{SD}}{dE} = \frac{8M_{det}t}{2J_A + 1} \frac{\rho_0}{M_\chi} (S_{00}(q)a_0^2 + S_{01}(q)a_0a_1 + S_{11}(q)a_1^2)I(E) \quad (65)$$

The form factors are calculated from detailed nuclear models including the momentum dependence. The list of SD form factors implemented in `micrOMEGAs` is given in the Appendix. For nuclei for which the form factor has not been computed precisely, we can describe the SD form factors with a Gauss distribution,

$$S_{ij}(q) = S_{ij}(0)\exp(-q^2R^2/4) \quad , \quad (66)$$

where $S_{ij}(0)$ is defined in Eq. 65 and S_p and S_n can be found in [44, 61]. To find out the effective nucleus radius to be used in the Gauss distribution, we perform a fit to the known form factors. First we observe that with a recoil energy $E = 15$ keV the form factors have a similar q dependence (within 10%),

$$\frac{S_{11}(q)}{S_{11}(0)} \approx \frac{S_{00}(q)}{S_{00}(0)} \approx \frac{S_{01}(q)}{S_{01}(0)}. \quad (67)$$

Thus, we can use the same effective radius for all form factors. To extract the A dependence of R we assume that Z exchange dominates, which means that S_{11} is the dominant form factor. We thus obtain

$$R_A = 1.7A^{1/3} - 0.28 - 0.78(A^{1/3} - 3.8 + \sqrt{(A^{1/3} - 3.8)^2 + 0.2}) \text{ fm} \quad (68)$$

A comparison between this approximate formula and the value extracted from the form factors tabulated in `micrOMEGAs` shows that the approximation works quite well, see Fig. 2. For light nuclei ($A < 100$), $R_A = 1.5A^{1/3}$ fm is also a very good approximate formula [67]. Some dependence on the DM model remains because of the different q behaviour of S_{ij} . This dependence has been shown to be small [66].

Table 3: Number of events per kg/day $\times 10^5$ for 5–50 keV recoil energy for SD interactions on various nuclei for model BP. Comparison between two sets of form factors and the Gauss approximation in eq. 66

	^{19}F	^{23}Na	^{27}Al	^{29}Si	^{39}K	^{73}Ge	^{93}Nb	^{125}Te	^{127}I	^{129}Xe	^{131}Xe
<i>Sxx</i> Tab.8	16.3	2.03	3.31	2.32	2.67	4.57	2.44	4.60	0.79	5.97	1.55
Gauss	16.4	2.05	3.36	2.26	2.70	4.67	2.50	4.68	0.75	6.25	1.46
<i>Sxx</i> Tab.9		2.13		2.32		7.92		5.54	1.27	4.37	1.37
Gauss		2.02		2.19		7.81		6.06	1.23	4.60	1.30

We compute the number of events for SD interactions for the nuclei listed in Table 3 in the region $5 < E < 50$ keV. For this we choose the sample model BP in Table 5 and compare the results using the precise form factors of Table 8 and Table 9 [65] with the ones obtained by using a Gauss distribution with the approximated formula Eq. 68 as well

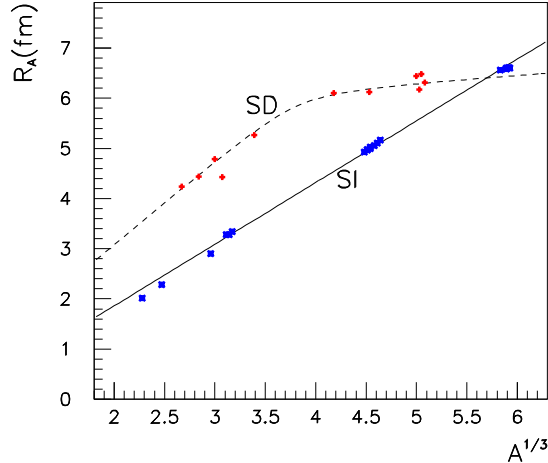


Figure 2: R_A for SI (full/blue) and SD (dotted/red) Gauss distribution form factors for various nuclei, the curves correspond to the approximations 60 and 68.

as the coefficients S_p and S_n in Eq. 65. We find that the approximate results with the Gauss distribution agree well with the exact form factors, the agreement is usually better than between different sets of form factors. Even for small nuclei where the interpolation for the radius R_A does not work as well there is a very good agreement between the different sets of form factors, see Table 3. This is because for light nuclei the momentum is very small hence the form factor does not need to be known precisely. Note that the Gauss approximation would not work as well at large recoil energies where the form factor decreases too rapidly.

5.3 Velocity distribution of dark matter

The nuclear recoil energy measured in direct detection experiments depends on the WIMP velocity distribution in the rest frame of the detector (55,65). This in turn depends on the WIMP velocity distribution in the rest frame of the galaxy and the Earth velocity with respect to this frame. The latter is determined from various observations. The measurements of the velocity of Sun and others objects close to the Sun give a value both for the velocity of rotation of the LSR(local standard of rest) [68]

$$v_0 = 220 \pm 20 km/s \quad (69)$$

and for the peculiar velocity of Sun in this system [69, 70] ⁶

$$\vec{v}_{pec} = (10.0, 5.2, 7.2) km/s \quad (70)$$

⁶Here we use the galactic co-ordinates (X,Y,Z) where X is toward the Galactic center, Y in the direction of rotation and Z toward the north Galactic pole.

The Earth velocity with respect to the galactic frame is thus the sum of $\vec{v}_0 = (0, v_0, 0)$, \vec{v}_{pec} and of the Earth velocity in the solar system. Assuming that the Earth's orbit is circular and that the axis of the ecliptic lies in the Y-Z plane, the Earth velocity in Galactic co-ordinates is

$$\vec{v}_e = v_e(-\sin(2\pi t), \sin\gamma\cos(2\pi t), \cos\gamma\cos(2\pi t)) \quad (71)$$

where $v_e = 29.79\text{km/s}$, $\gamma = 30.5^\circ$ and t is in years. More precise expressions, taking into account an elliptic orbit and the orientation of the axis of the ecliptic can be found in [71].

The velocity distribution of DM particles on the Earth is obtained from the DM velocity distribution in the rest frame of the Galaxy, F_{GRF} ,

$$f(v) = \int \delta(v - |\vec{V}|) F_{GRF}(\vec{V} - \vec{v}_0 - \vec{v}_{pec} - \vec{v}_e) d^3\vec{V} \quad (72)$$

Because the mass of Galaxy is finite there is some v_{max} such that $F_{GRF} = 0$ for $|\vec{V}| > v_{max}$, astronomical observations[72] give the 90% confidence interval

$$498\text{km/s} < v_{max} < 608\text{km/s}$$

with a median likelihood of $v_{max} = 544\text{km/s}$.

There are several models of DM velocity distribution[73], they are correlated with the DM density distribution. The simplest and most widely used model to describe the DM density is the isothermal sphere model [44]. In such a model the DM velocity distribution corresponds to a Maxwellian distribution. In our package we have implemented a truncated Maxwellian distribution,

$$F_{GRF}(\vec{V}) \sim \exp(-|\vec{V}|^2/\Delta V^2)\Theta(v_{max} - |\vec{V}|) \quad (73)$$

which leads to

$$f(v) = c_{\text{norm}} \left[\exp\left(-\frac{(v - v_1)^2}{\Delta V^2}\right) - \exp\left(-\frac{\min(v + v_1, v_{max})^2}{\Delta V^2}\right) \right] \quad (74)$$

where $\Delta V = v_0$ in the isothermal model, c_{norm} is fixed by the normalization condition

$$\int_0^\infty f(v) dv = 1$$

and

$$v_1 = |\vec{v}_0 + \vec{v}_{pec} + \vec{v}_e| \approx v_0 + (v_{pec})_y + v_e \sin\gamma\cos(2\pi t)$$

Note that the Earth motion around the Sun leads to a 7% modulation effect of v_1 and in turn to a modulation of the signal in direct detection experiments. This modulation was investigated in [71, 73] for a large set of models of DM spatial distributions. The DM velocity distribution close to the Sun could be quite different from the Maxwell distribution. For example condensation of cold DM in clumps and streams will lead to a delta-function distribution. This function has also been implemented in the code. The impact of the different velocity distributions on the limit on the detection rate of neutralinos was also discussed in [74]. In order to allow for deviations from the isothermal model, in the implementation of the Maxwellian distribution in `micrOMEGAs` we treat ΔV , ρ_0 , v_1 as free parameters. Furthermore alternative models for DM distribution can always be implemented by the user.

The DM density near the SUN is estimated to be in the range $\rho_0 = 0.1-0.7\text{ GeV/cm}^3$ [75]. As default, we take the commonly used value $\rho_0 = 0.3\text{ GeV/cm}^3$.

6 Description of routines

All routines are available both in C and Fortran and in both cases they have the same names and the same arguments. For simplicity, here we describe only C routines. The types of parameters are listed in

sources/micromegas.h for C routines and in sources/micromegas_f.h for Fortran routines.

- `setProtonFF(scalar, ps_vector, sigma)`
- `setNeutronFF(scalar, ps_vector, sigma)`

These two routines allow to redefine the default values of the coefficients describing the quark contents of nucleons, see Section 3.3. Each parameter is an array of type *double* of dimension 3 whose elements correspond to the form factors for *d*, *u*, and *s* quarks respectively. Default values of form factors are displayed in Table 4. To keep the default value for one set of coefficients, use NULL (NOFF in Fortran).

Table 4: Default values of quark form factors in proton and neutron.

current	proton			neutron		
	d	u	s	d	u	s
scalar	0.033	0.023	0.26	0.042	0.018	0.26
$\gamma_5 \gamma_\mu$	-0.427	0.842	-0.085	0.842	-0.427	-0.085
$\sigma_{\mu\nu}$	-0.23	0.84	-0.046	0.84	-0.23	-0.046

- `getScalarFF(m_u/m_d, m_s/m_d, sigma_piN, sigma_0, FF_proton, FF_neutron)`

This routine computes the scalar coefficients for quark contents in the nucleon from the mass ratios m_u/m_d , m_s/m_d as well as from $\sigma_{\pi N}$ and σ_0 following Eq. 27-29. It can be used to find the input values of the quark coefficients in `setProtonFF` and `setNeutronFF`. $\sigma_{\pi N}$ and σ_0 are specified in MeV. The coefficients are stored in `FF_proton` and in `FF_neutron`, both arrays of dimension 3 and of type *double*.

- `FeScLoop(sgn, mq, msq, mne)`

This function computes the loop K-factor for MSSM-like models, Eq. A-5 with a spin 1/2 WIMP and a scalar "squark". It allows to replace the denominators for *s*, *u*-channel diagrams as specified in eq. A-4. Here `mq`, `msq`, `mne` refer to quark, squark, and WIMP masses.

- `nucleonAmplitudes(qBOX, pAsi, pAsd, nAsi, nAsd)`

This routine calculates amplitudes for WIMP-nucleon elastic scattering at zero momentum. `pAsi`(`nAsi`) are spin independent amplitudes for protons(neutrons), whereas `pAsd`(`nAsd`) are the corresponding spin dependent amplitudes. Each of these four parameters is an array of type *double* and dimension 2. The first (zeroth) element of these arrays gives the χ -nucleon amplitudes whereas the second element gives $\bar{\chi}$ -nucleon amplitudes. Amplitudes are normalized such that the total cross section for either χ or $\bar{\chi}$ cross sections

$$\sigma_{tot} = \frac{4\mu_\chi^2}{\pi} (|A^{SI}|^2 + 3|A^{SD}|^2) \quad (75)$$

The `qBOX` parameter specifies a function like `FeScLoop()` that is used to improve the tree-level calculation in order to reproduce the results of the box-diagram calculation.

The function `FeScLoop` included in our package can be used for spin 1/2 WIMPS and scalar "squarks". To obtain the tree-level result, substitute `qBOX = NULL` (`qBOX = NoLoop`) in C(Fortran). `nucleonAmplitudes` returns a value different from zero only when there is an internal problem in calculation.

- `MSSMDDtest(loop, &pS,&pV,&nA,&nV)`

This routine computes the proton(neutron) scalar, $pS(nS)$ and vector, $pV,(nV)$ one-loop or tree-level amplitudes in the MSSM using directly the formulae of Drees and Nojiri [57]. If `loop = 0` then calculations are done at tree level assuming heavy quark condensates in the nucleon, otherwise the one-loop results for neutralino interactions with gluons are used. The QCD and SUSY-QCD corrections are included. Amplitudes are normalized according to (75). This routine exists only in the C-version.

- `fDvMaxwell(v)`

returns $f(v)/v$ where $f(v)$ is defined in Eq. (74). The argument v is expressed in km/s . This function is used as argument of the `nucleusRecoil` function described below.

- `SetfMaxwell(DV,v1,vmax)`

sets parameters for `fDvMaxwell`. The arguments correspond to the parameters ΔV , v_1 , and v_{max} in Eq. (74) in km/s units. Unless this routine is called the program uses the default values (220,225.2,700).

- `SetfDelts(v)`

sets velocity of DM for δ -function distribution.

- `fDvDelts(v)`

indicates to `nucleusRecoil` that the velocity distribution is a delta function which is non-zero for the parameter specified in `SetfDelts(v)`.

- `SetFermi(C,B,a)` sets parameters for A-dependence of the Fermi half radius, $R_A = CA^{1/3} + B$ and for the surface thickness, a . Default values are given in Eq. 60.

- `nucleusRecoil(rho,fDv,A,Z,J,S00,S01,S11,qBOX,dNdE)`

This is the main routine of the direct detection module. The input parameters `rho`, `fDv`, specify the DM velocity distribution while A , Z , J , $S00$, $S01$, $S11$ specify properties of detector material. The return value gives the number of events per day and per kilogram of detector material. The distribution over recoil energy is stored in the array $dNdE$. This array has to be of type *double* with 200 elements. The value in the i^{th} element corresponds to

$$\left. \frac{dN}{dE} \right|_{E=i*keV}$$

in units of (1/keV/kg/day). For a complex WIMP, `nucleusRecoil` averages over WIMP and $\overline{\text{WIMP}}$.

The input parameters are:

`rho` - density of DM near the Earth in GeV/cm^3 ;

`fDv` - this parameter is a function which specifies the DM velocity distribution, `fDv`= $f(v)/v$ where $f(v)$ is defined in Eq.(72), the velocity v is given in km/s and `fDv(v)` in $(s/km)^2$. The function `fDvMaxwell` described above is the default function that can be used here.

`A` - Atomic number of nucleus;

`Z` - Number of protons in the nucleus;

`J` - nucleus spin.

`qBOX` - a parameter needed by `nucleonAmplitudes`, see the description above.

$S00(p)$, $S01(p)$, $S11(p)$ are nucleus form factors for spin-dependent interactions. They

are functions of the momentum transfer in fm^{-1} (argument of *double* type). These form factors are assumed to be normalized as in Eq. 65.

Nucleus form factors for a wide set of nuclei are implemented in `micrOMEGAs`. The available form factors are listed in Tables 8, 9 in Appendix B and are extracted from the review article of Bednyakov and Simkovic [65]. These functions are named

$$S\{xx\}\{Nucleus\ Name\}\{Atomic\ Number\}[A] \quad (76)$$

where xx is either 00,11 or 01. The last character is optional and is used to distinguish different implementations of form factor for the same isotope.

For convenience our package has predefined constants for nucleus charge

$$Z_{\{Name\}}$$

and nucleus spin

$$J_{\{Name\}}\{atomic_number\}$$

for all isotopes listed in Tab.8,9.

For example, a call to `nucleusRecoil` for ^{73}Ge detector should be

```
N=nucleusRecoil(0.3,fDvMaxwell,73,Z_Ge,J_Ge73,S00Ge73,S01Ge73,S11Ge73,FeScLoop,dNdE);
```

- `int PlotSS(Sxx,A, title, Emax)`

allows a visual check of the spin dependent form factors. This routine opens a new window where `Sxx` is displayed as function of the recoil energy. Here `Sxx` stands for any of functions in Tab. 8, 9, `A` is the atomic number, `title` defines the text that will be displayed on the screen and `Emax` is the upper limit of the recoil energy for the plot.

The `PlotSS` routine is based on CalcHEP [76] plot facilities. By a click of the mouse on one point in the plot area one gets information about the value of X/Y coordinates for that point. To close the window press the '*Esc*' key. Pressing some other key opens the menu which displays `min` and `max` values of the function and allows to change limits of the Y axis and switch between linear/logarithmic scale of Y axis. For additional help press the F1 key.

- `nucleusRecoil0(0.3,fDv,A,Z,J,Sp,Sn,qBOX,dNdE)`

is similar to the function `nucleusRecoil` except that it uses Eq. 64 to define $S00(0)$, $S11(0)$, $S01(0)$ and the q-dependence of these form factors is the one associated with the Fermi distribution with radius, R_A given in Eq. 68. This function can for example be used for light nuclei, such as 3He , or for any other nuclei where the more precise form factor has not been included in Tab. 8. For all nuclei listed in Tab. 8 as well as for 1H ($S_p = 0.5, S_n = 0$) and $^3He[100]$, form factors have been predefined with names

$$Sp\{Nucleus\ Name\}\{Atomic\ Number\} \quad \text{and} \quad Sn\{Nucleus\ Name\}\{Atomic\ Number\} \quad (77)$$

These constants correspond to the form factors listed in Tab.8 extracted from the review article [61]. They all satisfy Eq.64. Table 3 shows how well the approximation works.

Two auxiliary routines are provided to work with the energy spectrum computed with `nucleusRecoil` and `nucleusRecoil0`.

- `displayRecoilPlot(dNdE,title,E1,E2)`

plots the generated energy distribution `dNdE`. Here `title` is a character string specifying

the title of the plot and $E1, E2$ are minimal and maximal values for the displayed energy. $E1, E2$ have to be an integer value in keV units, $E2$ has to be smaller than 200. This routine has the same service facilities as `PlotSS` described above. Note that the plots can be saved in Latex format as well as in GNU PLOT or PAW formats.

• `cutRecoilResult(dNdE, E1, E2)`

calculates the number of events in an energy interval defined by values $E1, E2$ in keV units.

7 Sample results

Table 5: SI and SD cross sections in sample SUGRA models.

	AP	BP	CP	DP	IP	KP	MP	NUG	NUH
m_0	130	70	90	120	180	2500	1100	1620	250
$M_{1/2}$	600	250	400	500	350	550	1100	300	530
A_0	0	-300	0	-400	0	-80	0	0	0
$\tan\beta$	5	10	10	10	35	40	50	10	30
μ	+	+	+	-	+	-	+	+	+
Masses									
$\tilde{\chi}_1^0$	248.4	97.9	161.7	207.4	141.3	223.5	476.3	109.4	218.6
$\tilde{\chi}_1^+$	466.8	183.0	302.6	395.7	264.4	284.1	893.3	156.7	404.3
\tilde{l}_1	257.1	107.6	170.5	213.8	152.3	2129.	816.7	1607.	254.4
\tilde{t}_1	952.9	362.5	649.9	774.6	581.8	1730.	1836.	999.3	848.2
h	111.5	111.0	112.5	114.2	112.4	118.6	119.2	113.7	115.3
A	888.2	420.5	576.4	769.0	426.2	1547.6	927.4	1614.	497.8
Ωh^2	0.126	0.101	0.115	0.107	0.113	0.101	0.128	0.119	0.088
$\sigma_p^{SI} \times 10^9 \text{pb}$									
set A	0.98	7.50	2.48	0.019	19.6	9.03	0.509	46.9	7.65
set B	1.82	15.9	4.98	0.055	44.1	14.4	1.06	85.7	16.7
set C	0.77	5.49	1.87	0.011	13.9	7.67	0.375	37.2	5.50
$\sigma_p^{SD} \times 10^6 \text{pb}$									
set A'	0.301	5.00	1.97	0.360	3.78	140.	0.096	510.	2.22
set B'	0.230	3.69	1.56	0.261	3.05	129.	0.082	470.	1.89
$\sigma_n^{SD} \times 10^6 \text{pb}$									
set A'	0.251	4.34	1.55	0.322	2.89	87.0	0.069	317.	1.58
set B'	0.334	5.89	2.01	0.443	3.69	99.1	0.085	362.	1.93
$N \times 10^3 / \text{kg/day}$									
^{73}Ge	0.19	3.00	0.70	0.0071	6.08	2.41	0.056	20.3	1.68
^{131}Xe	0.31	5.35	1.18	0.0085	10.5	3.36	0.089	31.6	2.79

The predictions for the spin independent cross sections on protons and spin dependent cross sections on neutrons and protons are listed in Table 5 in the case of the MSSM with input parameters fixed at the GUT scale. The first seven models (AP to MP) are inspired by the mSUGRA benchmarks of Ref. [101]. The input parameters have been modified such

that the prediction for Ωh^2 falls near the central WMAP value when the top quark mass is fixed to the value measured at Tevatron, $m_t = 171.4$ GeV [102]. The parameters of Model BP were adjusted to the ones of the SPA1A benchmark [103]. The spectrum calculator used is SuSPECT [104]. The last two models are non-universal SUGRA models. In model NUG, the gaugino masses are non-universal at the GUT scale with $M_3 = 0.7M_2 = 0.7M_1$ leading to a lighter coloured sector than in the universal case. In model NUH only the Higgs masses are non-universal with $M_{H_u} = 2m_0$ and $M_{H_d} = -0.6m_0$. For each model the predictions for the SI cross section are given for three sets of values for the coefficients describing the quark density contents in the nucleon. Set A correspond to the default values, Eq. 35, while the input parameters for set B ($\sigma_{\pi N} = 70, \sigma_0 = 35$ MeV) and set C ($\sigma_{\pi N} = 55, \sigma_0 = 40$ MeV) are varied within the expected range, Eq. 29. Note that these do not correspond to the most extreme choices, yet the predictions for the cross sections can vary by a factor of 2 or 3. For the SD cross sections, set A' and set B' correspond respectively to the old (Eq. 39) and new (Eq. 40) estimates of the quark density coefficients. In Table 5 the predictions for the number of events per day and per kg of detector material for ^{73}Ge and ^{131}Xe are also presented. Here we assume the default values for the quark density coefficients as well as for the velocity distribution. The distribution of the number of events as function of the energy is also computed. The results for models BP and KP for a detector made of ^{131}Xe are displayed in Fig. 3.

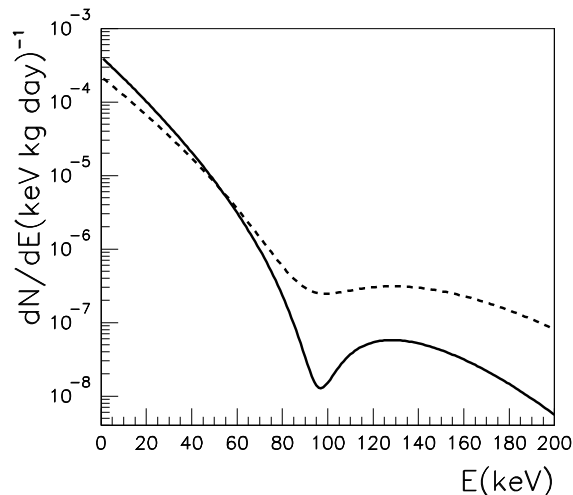


Figure 3: dN/dE for a ^{131}Xe detector in two mSUGRA models specified in Table 5, BP (full) and KP (dash).

We have also compared our results with other public codes. For this we have used the same spectrum calculator (here we have taken Isajet_7.75) and have removed from micrOMEGAs the QCD and SUSY QCD corrections which are neglected in other codes. For a given set of quark coefficients, our results for σ^{SI} are in very good agreement with Isajet_7.75 for the dominant contribution due to Higgs exchange, differences appear in the squark exchange contribution. For SUGRA models this can lead to 25% differences between the two codes. For σ^{SD} , our prediction is usually below the one of Isajet, differences between the two codes can reach a factor 4. This can be traced back to a sign discrepancy

between the Z and the squark exchange diagram ⁷. As concerns DarkSUSY_4.1, we have discrepancies that can reach 25% for σ^{SI} , this is due to the Higgs exchange diagram. In DarkSUSY the running mass is used in the hqq vertex while the pole mass is used when estimating the quark scalar coefficient, whereas in micrOMEGAs we use the same mass everywhere as we have discussed in Section 3.3. Our predictions for σ^{SD} are in very good agreement with those of DarkSUSY for the Z exchange contribution. We however have a factor 2 difference in the squark exchange diagram which can lead to 50% discrepancies in σ^{SD} for our SUGRA test models. Increasing the squark exchange contribution by a factor 2 in DarkSUSY, we recover very good agreement with micrOMEGAs ⁸.

Table 6: Comparison with Isajet_7.75 and DarkSUSY_4.1 in sample mSUGRA models

	AP	BP	CP	DP	IP	MP
m_0	130	70	90	120	180	1100
$M_{1/2}$	600	250	400	500	350	1100
A_0	0	-300	0	-400	0	0
$\tan \beta$	5	10	10	10	35	50
μ	+	+	+	-	+	+
$\sigma_p^{SI} \times 10^9 \text{pb}$						
micrOMEGAs	0.466	3.65	1.17	0.0067	9.57	0.16
Isajet	0.448	2.85	1.01	0.0025	7.18	0.14
Isajet'	0.460	3.64	1.16	0.0067	9.45	0.16
Darksusy	0.357	2.89	0.895	0.0054	7.54	0.118
$\sigma_p^{SD} \times 10^6 \text{pb}$						
micrOMEGAs	0.248	4.44	1.66	0.306	3.19	0.068
Isajet	0.87	16.7	4.72	1.37	8.16	0.141
Isajet'	0.241	4.31	1.62	0.297	3.11	0.067
DarkSUSY	0.370	6.79	2.29	0.506	4.21	0.082
DarkSUSY'	0.252	4.49	1.68	0.315	3.19	0.067
$\sigma_n^{SD} \times 10^6 \text{pb}$						
micrOMEGAs	0.203	3.75	1.29	0.267	2.41	0.0489
Isajet	0.45	8.49	2.49	0.694	4.35	0.077
Isajet'	0.198	3.66	1.26	0.260	2.36	0.0478
DarkSUSY	0.254	4.71	1.54	0.353	2.80	0.054
DarkSUSY'	0.201	3.70	1.27	0.266	2.36	0.047

In the sample models of Table 7 the dependence on the axial vector coefficients for the spin dependent cross-section is far less important (within 30% between sets A' and B') than for the scalar cross section. Furthermore much smaller variations are observed if one just sticks to the uncertainty associated with the latest experimental results, Eq. 40. This is specific to SUGRA models where one finds that the Z exchange diagram completely dominates over the squark exchange diagram. This is valid in all models where Z exchange

⁷The direct detection module is being improved in Isajet, we expect much better agreement between the two codes in the next public version, Isajet_7.76 [105].

⁸The DarkSUSY code has been updated and is now in good agreement with micrOMEGAs [106]

Table 7: SI and SD cross sections on protons in non-SUGRA models, all masses in GeV.

	MSSM1	LH	RHN1	RHN2
	$M_1 = 200$ $M_2 = 400$ $\mu = 350$ $m_{\tilde{q}_R} = 300$ $m_{\tilde{t}_R} = 200$ $\tan \beta = 10$	$f = 1000$ $M_H = 220$ $\kappa = 1$ $\kappa_1 = 0.5$ $\sin \alpha = \frac{1}{\sqrt{2}}$	$g_Z = 0.002$ $g_H = 0.025$ $M_{Z'} = 5000$ $M_{\nu_R} = 46.$ $M_H = 200.$	$g_Z = 0.0066$ $g_H = 0.025$ $M_{Z'} = 5000$ $M_{\nu_R} = 900.$ $M_H = 200.$
Masses (GeV)				
χ	193.2	150.2	46.	900.
\tilde{l}_1	204.7	701.7	5000.	5000.
\tilde{t}_1	326.6	991.9	5000.	5000.
h	115.6	220.0	200.	200.
Ωh^2	0.100	0.109	0.100	0.151
$\sigma_n^{SI} \times 10^9 pb$				
A	18.9	0.33	47.9	584.
B	38.7	0.60	46.2	578.
C	14.2	0.27	48.4	586.
$\sigma_p^{SD} \times 10^6 pb$				
A'	0.47	3.1×10^{-6}	0.317	3.59
B'	0.039	6.5×10^{-6}	0.293	3.31
$\sigma_n^{SD} \times 10^6 pb$				
A'	3.17	2.7×10^{-8}	0.197	2.22
B'	7.21	3.7×10^{-7}	0.224	2.53

dominates. In the more general MSSM with weak scale input parameters, it is possible to find models where the squark exchange diagrams contribute significantly to the spin dependent cross section and can furthermore interfere with the Z exchange diagram. This can lead to a strong reduction of either the proton or neutron cross section as shown for a sample MSSM model in Table 7 where the most relevant parameters are specified in the Table, in addition we set $m_{\tilde{q}_L} = M_A = -A_t = 1$ TeV, $m_{\tilde{l}_L} = 500$ GeV and $M_3 = 800$ GeV. Finally sample results for the case of a gauge boson in the Little Higgs model (LH)⁹ and of a Dirac right-handed neutrino (RHN1 and RHN2) are listed in Table 7. Note that in this table the values for SI cross sections on neutrons only are given, in most models these numbers are similar to the ones of protons except in the RH neutrino model where the cross section on protons is very much suppressed. In this model the small dependence on the quark coefficients is due to the Higgs exchange diagram. The results for the RH neutrino model agree with the ones of [38].

⁹We use the version of the Little Higgs model implemented into CalcHEP and available at <http://hep.pa.msu.edu>, more details can be found in [107].

8 Installation

The package can be obtained from the web page www.lapp.in2p3.fr/lapth/micromegas. All instructions for installing the package can be found in [108]. Contrary to previous versions, the user must download only one file `micromegas_2.2.tgz` which contains the full implementation of different models such as the MSSM, CPV-MSSM [109], NMSSM [110],[111] as well as the little Higgs model (LHM) [107] and the right-handed neutrino model(RHNM) [38]. Facilities to incorporate other new models remain as in `micrOMEGAs_2.0`, specific instructions on how to install new models are given in [108]. Note that the identifiers `S0` and `V5` are now reserved for the auxiliary fields used to generate automatically the operators in Table 1, they cannot be used to designate particles in the model. Note also that since `micrOMEGAs` searches for quarks in the list of particles by identifying the PDG codes, care has to be taken to implement these correctly in the model file. The direct detection module is not compatible with earlier versions of the supersymmetric models, since light quark masses and the corresponding couplings of light quarks to Higgses need to be introduced. To run the code we provide for each model one sample file, `main.c` (`main.F` in Fortran). This sample program can be used to compute the relic density of DM, the cross sections for direct and indirect detection, the cross sections at colliders and decay widths. Various options can be set in that program depending on the need of the user, the various switches available are commented in the main file. The sample programs `cycle2.c` and `cycle5.c` found in the MSSM directory will reproduce the numerical results in Tables 2,5.

9 Summary

The new module for computation of the cross-section for WIMP scattering on nucleus in `micrOMEGAs` described here applies to any type of CDM candidate, whether Majorana or Dirac fermion, scalar or vector boson. After the new model is implemented within `micrOMEGAs`, the mass, the spin and the interactions of the WIMP candidate are computed automatically. Because the nucleon has an important light quarks component, WIMP interactions with light quarks in the nuclei often dominate over those of heavy quarks. For scalar interactions the amplitude for WIMP quark scattering is proportional to the quark mass, thus the mass of light quarks have to be taken into account and incorporated into the model file. In the specific case of the MSSM this means expanding the model file since for the relic density calculation all fermions of the first two generations were taken to be massless. Furthermore within this model, higher-order corrections to the $H\bar{q}q$ vertices for down-type quarks such as SUSY-QCD corrections are taken into account. For all models, we use an effective vertex for WIMP interactions with heavy quark in the nuclei, this takes into account dominant QCD corrections to Higgs exchange diagrams. A more precise treatment is available for MSSM-like models.

We have also explicitly shown on a few examples the impact of varying the coefficients for the quark density content of the nucleon. Uncertainties are very large for scalar interactions and are in general more under control for spin dependent interactions that arise through Z exchange. For other contributions to spin dependent interactions the uncertainties can be quite large although the value predicted is often several orders of magnitude below the present limit.

10 Acknowledgements

We thank A. Djouadi and E. Pilon for clarifications on QCD corrections, V. Shevchenko for discussions on the tensor quark coefficients, A. Bednyakov for discussions on the nuclear form factors and A. Belyaev for providing the CalCHEP code for the little Higgs model and for discussions on the micrOMEGAs-Isajet comparison. We also thank S. Kraml for testing various parts of our code. Part of this work was performed during the CERN Theory Institute on "LHC-Cosmology Interplay", A.P. and G.B. thank the organisers for their warm hospitality. This work was supported in part by the GDRI-ACPP of CNRS and by the French ANR project ToolsDmColl, BLAN07-2-194882. The work of A.P. was supported by the Russian foundation for Basic Research, grants RFBR-08-02-00856-a, RFBR-08-02-92499-a.

Note added

An online tool for computation of direct detection rates with micrOMEGAs 2.2 has been set up by Rachid Lemrani, see http://pisrv0.pit.physik.uni-tuebingen.de/darkmatter/micromegas_g/.

Appendix A - Box diagrams

As shown explicitly by Dress and Nojiri, the tree-level calculation overestimates s-channel amplitudes when $M_{\tilde{q}} - M_\chi < m_q$. In that case one should instead compute completely the box diagrams or use the procedure described here. In the MSSM, the Lagrangian for neutralino-quark-squark interaction has the generic form

$$\mathcal{L}_Y = \bar{q}(a + b\gamma_5)\chi\tilde{q} + h.c. \quad (\text{A-1})$$

and leads to the WIMP-quark scattering amplitude at tree-level

$$A = \frac{1}{4} \left(\frac{b^2}{M_{\tilde{q}}^2 - (M_\chi + m_q)^2} - \frac{a^2}{M_{\tilde{q}}^2 - (M_\chi - m_q)^2} \right) \quad (\text{A-2})$$

The explicit computation of the box diagram [57] leads to an amplitude of the form

$$A_{box} = \frac{1}{4} \left((b^2 - a^2)F_D(m_q, M_{\tilde{q}}, M_\chi) + (a^2 + b^2)F_S(m_q, M_{\tilde{q}}, M_\chi) \right) \quad (\text{A-3})$$

where F_D and F_S are loop functions. A simple modification of the propagators in A-2 will therefore reproduce the amplitude A_{box} ,

$$\frac{1}{M_{\tilde{q}}^2 - (M_\chi \pm m_q)^2} \rightarrow K(\pm 1, m_q, M_{\tilde{q}}, M_\chi) \quad (\text{A-4})$$

where

$$\begin{aligned} K(s, m_q, M_{\tilde{q}}, M_\chi) &= F_D(m_q, M_{\tilde{q}}, M_\chi) + sF_S(m_q, M_{\tilde{q}}, M_\chi) \\ &= \frac{3}{2}m_q(m_q I_1 - \frac{2}{3}M_\chi^2 I_3 - sM_\chi(I_2 - \frac{1}{3}I_5 - \frac{2}{3}M_\chi^2 I_4)) \end{aligned} \quad (\text{A-5})$$

and

$$I_1 = \int_0^1 dx \frac{x^2 - 2x + 2/3}{D^2} \quad (\text{A-6})$$

$$I_2 = \int_0^1 dx \frac{x(x^2 - 2x + 2/3)}{D^2} \quad (\text{A-7})$$

$$I_3 = \int_0^1 dx \frac{x^2(1-x)^2}{D^3} \quad (\text{A-8})$$

$$I_4 = \int_0^1 dx \frac{x^3(1-x)^2}{D^3} \quad (\text{A-9})$$

$$I_5 = \int_0^1 dx \frac{x(1-x)(2-x)}{D^2} \quad (\text{A-10})$$

$$D = x^2 M_\chi^2 + x(M_{\tilde{q}}^2 - m_q^2 - M_\chi^2) + m_q^2 \quad (\text{A-11})$$

The modification of the denominators of tree level diagrams in micrOMEGAs is achieved by a small modification of the CalcHEP code. Obviously this trick will work in any MSSM-like model where the WIMP is a fermion that interacts with quarks via scalar quarks, in particular in the NMSSM and the CPV-MSSM. The same trick can be generalized to other models, for this however one has to compute the appropriate loop factors which depend on the WIMP and 'squark' spin. Note that the box diagrams for WIMP scattering on gluons includes also diagrams where gluons couple to squarks. When the WIMP scattering amplitude is computed with the loop K-factor option, micrOMEGAs omits the tree-level processes involving squarks (or in general colored triplet that are not quarks) assuming that their contributions are included in the K-factor.

Appendix B - Spin dependent nucleus form factors

Table 8: Nucleus SD form factors realized in micrOMEGAs

Identifier	Isotope	Ref	data in [65]	comments
SxxF19	^{19}F	[112]	Eq. 7	
SxxSi29	^{29}Si	[112]	Eq. 14	
SxxNa23	^{23}Na	[66]	Eq. 9	
SxxTe125	^{125}Te	[66]	Eq. 18, Tab. IV	Bonn-A potential
SxxI127	^{127}I	[66]	Eq. 20	Bonn-A potential
SxxXe129	^{129}Xe	[66]	Eq. 21 Tab. IX	Bonn-A potential
SxxXe131	^{131}Xe	[66]	Eq. 21 Tab. IX	Bonn-A potential
SxxAl27	^{27}Al	[113]	Eq. 11	
SxxK39	^{39}K	[113]	Eq. 15	
SxxGe73	^{73}Ge	[114]	Eq. 17	
SxxNb92	^{93}Nb	[115]	Tab. II	Scanned plot

Table 9: Alternative nucleus SD form factors.

Identifier	Isotope	Ref	data in [65]	comments
SxxSi29A	^{29}Si	[116]	Eq. 12	
SxxNa23A	^{23}Na	[112]	Eq. 10	
SxxTe125A	^{125}Te	[66]	Eq. 18, Tab.IV	Nijmegen II potential
SxxI127A	^{127}I	[66]	Eq. 19, Tab.VI	Nijmegen II potential
SxxXe129A	^{129}Xe	[66]	Eq. 21 Tab. IX	Nijmegen II potential
SxxXe131A	^{131}Xe	[66]	Eq. 21 Tab. IX	Nijmegen II potential
SxxGe73A	^{73}Ge	[116]	Eq. 16	
SxxXe131B	^{131}Xe	[117]	TABLE VII	$S_{00}^{131}(0)$ should be 0.04^{10}

Appendix C - Additional routines

To facilitate model independent comparisons with data, we provide additional routines to compute the nucleus recoil energy using as input the WIMP mass and the cross sections for SI and SD scattering on nucleons.

- `nucleusRecoilAux(rho, fDv, A, Z, J, S00, S01, S11, Mwimp, csIp, csIn, csDp, csDn, dNdE)`

This function is similar to `nucleusRecoil` and returns the number of events per day and per *kg* of detector material. The additional input parameters include the WIMP mass, `csIp(csIn)` the SI cross sections for WIMP scattering on protons (neutrons) and `csDp(csDn)` the SD cross sections for protons(neutrons). A negative value for one of these cross sections corresponds to a destructive interference between proton and neutron amplitudes.

- `nucleusRecoil0Aux(rho, fDv, A, Z, J, Sp, Sn, Mwimp, csIp, csIn, csDp, csDn, dNdE)`

This function is similar `nucleusRecoilAux` except that it uses Eq. 64 to define $S_{00}(0)$, $S_{11}(0)$, $S_{01}(0)$. For details see the description of `nucleusRecoil0`.

- `setRecoilEnergyGrid(step, nStep)`

This function redefines the grid for the recoil energy. After calling this function the `nucleusRecoil` function returns a recoil energy distribution where $E_i = i \times \text{step}$ keV, $i = 0, \dots, \text{nStep} - 1$.

References

- [1] M. Tegmark *et. al.*, *Phys. Rev.* **D74** (2006) 123507, [[astro-ph/0608632](#)].
- [2] D. N. Spergel *et. al.*, **WMAP** Collaboration *Astrophys. J. Suppl.* **170** (2007) 377, [[astro-ph/0603449](#)].
- [3] G. Bertone, D. Hooper, and J. Silk, *Phys. Rept.* **405** (2005) 279–390, [[hep-ph/0404175](#)].
- [4] H. Goldberg, *Phys. Rev. Lett.* **50** (1983) 1419.
- [5] J. R. Ellis, J. S. Hagelin, D. V. Nanopoulos, K. A. Olive, and M. Srednicki, *Nucl. Phys.* **B238** (1984) 453–476.

- [6] D. Hooper and S. Profumo, [hep-ph/0701197](#).
- [7] H.-C. Cheng, K. T. Matchev, and M. Schmaltz, *Phys. Rev.* **D66** (2002) 036005, [[hep-ph/0204342](#)].
- [8] G. Servant and T. M. P. Tait, *New J. Phys.* **4** (2002) 99, [[hep-ph/0209262](#)].
- [9] K. Agashe and G. Servant, *Phys. Rev. Lett.* **93** (2004) 231805, [[hep-ph/0403143](#)].
- [10] J. Hubisz and P. Meade, *Phys. Rev.* **D71** (2005) 035016, [[hep-ph/0411264](#)].
- [11] V. Barger *et. al.*, *Phys. Rev.* **D75** (2007) 115002, [[hep-ph/0702036](#)].
- [12] M. Cvetič, D. A. Demir, J. R. Espinosa, L. L. Everett, and P. Langacker, *Phys. Rev.* **D56** (1997) 2861–2885, [[hep-ph/9703317](#)].
- [13] J. McDonald, *Phys. Rev.* **D50** (1994) 3637–3649, [[hep-ph/0702143](#)].
- [14] R. Barbieri, L. J. Hall, and V. S. Rychkov, *Phys. Rev.* **D74** (2006) 015007, [[hep-ph/0603188](#)].
- [15] R. Lemrani, **EDELWEISS** Collaboration *Phys. Atom. Nucl.* **69** (2006) 1967–1969.
- [16] R. Bernabei *et. al.*, *AIP Conf. Proc.* **878** (2006) 91–98.
- [17] D. S. Akerib *et. al.*, **CDMS** Collaboration [astro-ph/0609189](#).
- [18] J. Angle *et. al.*, **XENON** Collaboration [arXiv:0706.0039](#) [[astro-ph](#)].
- [19] Z. Ahmed *et al.* [CDMS Collaboration], [arXiv:0802.3530](#) [[astro-ph](#)].
- [20] T. Sumner, **UKDMC** Collaboration *PoS HEP2005* (2006) 003.
- [21] N. Ferrari, **Warp** Collaboration *J. Phys. Conf. Ser.* **39** (2006) 111–113.
- [22] J. Lee, *AIP Conf. Proc.* **878** (2006) 106–110.
- [23] Y. D. Kim, **XMASS** Collaboration *Phys. Atom. Nucl.* **69** (2006) 1970–1974.
- [24] J. A. Nikkel, W. H. Lippincott, and D. N. McKinsey, *Int. J. Mod. Phys.* **A20** (2005) 3113–3114.
- [25] M. Laffranchi and A. Rubbia, **ArDM** Collaboration [hep-ph/0702080](#).
- [26] H. Kraus *et. al.*, *J. Phys. Conf. Ser.* **39** (2006) 139–141.
- [27] T. Morlat *et. al.*, [arXiv:0704.2037](#) [[astro-ph](#)].
- [28] F. Aubin *et. al.*,. Prepared for 9th ICATPP Conference on Astroparticle, Particle, Space Physics, Detectors and Medical Physics Applications, Villa Erba, Como, Italy, 17-21 Oct 2005.
- [29] Y. Inoue *et. al.*,. Prepared for Origin of Matter and the Evolution of Galaxies (OMEG03), RIKEN, Wako, Saitama, Japan, 17-19 Nov 2003.

- [30] G. J. Alner *et al.*, **UK Dark Matter** Collaboration *Phys. Lett.* **B616** (2005) 17–24, [[hep-ex/0504031](#)].
- [31] H. S. Lee *et al.* [KIMS Collaboration], *Phys. Rev. Lett.* **99** (2007) 091301 [[arXiv:0704.0423](#) [[astro-ph](#)]].
- [32] D. Santos and E. Moulin, [astro-ph/0412273](#).
- [33] C. B. Winkelmann, J. Elbs, E. Collin, Y. M. Bunkov, and H. Godfrin, *Nucl. Instrum. Meth.* **A559** (2006) 384–386.
- [34] R. Bernabei *et al.*, *Riv. Nuovo Cim.* **26N1** (2003) 1–73, [[astro-ph/0307403](#)].
- [35] C. Savage, P. Gondolo, and K. Freese, *Phys. Rev.* **D70** (2004) 123513, [[astro-ph/0408346](#)].
- [36] J. Ellis, T. Hahn, S. Heinemeyer, K. A. Olive, and G. Weiglein, *JHEP* **10** (2007) 092, [[arXiv:0709.0098](#) [[hep-ph](#)]].
- [37] R. Trotta, R. Ruiz de Austri, and L. Roszkowski, *J. Phys. Conf. Ser.* **60** (2007) 259–263.
- [38] G. Bélanger, A. Pukhov, and G. Servant, [arXiv:0706.0526](#) [[hep-ph](#)].
- [39] D. S. Akerib *et al.*, *Nucl. Instrum. Meth.* **A559** (2006) 411–413.
- [40] J. Angle *et al.*, [arXiv:0805.2939](#) [[astro-ph](#)].
- [41] G. J. Alner *et al.*, **ZEPLIN-II** Collaboration *Phys. Lett.* **B653** (2007) 161–166, [[arXiv:0708.1883](#) [[astro-ph](#)]].
- [42] D. S. Akerib *et al.*, **CDMS** Collaboration *Phys. Rev.* **D73** (2006) 011102, [[astro-ph/0509269](#)].
- [43] S. Desai *et al.* [Super-Kamiokande Collaboration], *Phys. Rev. D* **70** (2004) 083523 [Erratum-*ibid.* **D 70** (2004) 109901] [[arXiv:hep-ex/0404025](#)].
- [44] G. Jungman, M. Kamionkowski, and K. Griest, *Phys. Rept.* **267** (1996) 195–373, [[hep-ph/9506380](#)].
- [45] C. Munoz, *Int. J. Mod. Phys.* **A19** (2004) 3093–3170, [[hep-ph/0309346](#)].
- [46] A. Birkedal, A. Noble, M. Perelstein, and A. Spray, *Phys. Rev.* **D74** (2006) 035002, [[hep-ph/0603077](#)].
- [47] K. Agashe and G. Servant, *JCAP* **0502** (2005) 002, [[hep-ph/0411254](#)].
- [48] L. Lopez Honorez, E. Nezri, J. F. Oliver, and M. H. G. Tytgat, *JCAP* **0702** (2007) 028, [[hep-ph/0612275](#)].
- [49] C. Arina and N. Fornengo, [arXiv:0709.4477](#) [[hep-ph](#)].
- [50] H. Baer, C. Balazs, A. Belyaev, and J. O’Farrill, *JCAP* **0309** (2003) 007, [[hep-ph/0305191](#)].

- [51] J. R. Ellis, K. A. Olive, Y. Santoso, and V. C. Spanos, *Phys. Rev.* **D71** (2005) 095007, [hep-ph/0502001].
- [52] J. R. Ellis, A. Ferstl, and K. A. Olive, *Phys. Lett.* **B481** (2000) 304–314, [hep-ph/0001005].
- [53] E. Accomando, R. Arnowitt, B. Dutta, and Y. Santoso, *Nucl. Phys.* **B585** (2000) 124–142, [hep-ph/0001019].
- [54] A. Bottino, F. Donato, N. Fornengo, and S. Scopel, *Phys. Rev.* **D63** (2001) 125003, [hep-ph/0010203].
- [55] Y. G. Kim, T. Nihei, L. Roszkowski, and R. Ruiz de Austri, *JHEP* **12** (2002) 034, [hep-ph/0208069].
- [56] U. Chattopadhyay, A. Corsetti, and P. Nath, *Phys. Rev.* **D68** (2003) 035005, [hep-ph/0303201].
- [57] M. Drees and M. Nojiri, *Phys. Rev.* **D48** (1993) 3483–3501, [hep-ph/9307208].
- [58] P. Gondolo *et. al.*, *JCAP* **0407** (2004) 008, [astro-ph/0406204].
- [59] G. Bélanger, F. Boudjema, A. Cottrant, A. Pukhov, and A. Semenov, *Nucl. Phys.* **B706** (2005) 411–454, [hep-ph/0407218].
- [60] T. Falk, A. Ferstl, and K. A. Olive, *Astropart. Phys.* **13** (2000) 301–316, [hep-ph/9908311].
- [61] V. A. Bednyakov and F. Simkovic, *Phys. Part. Nucl.* **36** (2005) 131–152, [hep-ph/0406218].
- [62] G. Fricke *et al.*, *Atomic Data and Nuclear Data Tables* **60** (1995) 177.
- [63] H. de Vries, C. W. de Jaeger, C. de Vries, *Atomic Data and Nuclear Data Tables* **36** (1987) 495.
- [64] J. D. Lewin and P. F. Smith, *Astropart. Phys.* **6** (1996) 87–112.
- [65] V. A. Bednyakov and F. Simkovic, *Phys. Part. Nucl.* **37** (2006) S106–S128, [hep-ph/0608097].
- [66] M. T. Ressell and D. J. Dean, *Phys. Rev.* **C56** (1997) 535–546, [hep-ph/9702290].
- [67] J. R. Ellis and R. A. Flores, *Phys. Lett. B* **263** (1991) 259.
- [68] F. J. Kerr and D. Lynden-Bell, *Mon. Not. Roy. Astron. Soc.* **221** (1986) 1023.
- [69] W. Dehnen and J. Binney, *Mon. Not. Roy. Astron. Soc.* **298** (1998) 387–394, [astro-ph/9710077].
- [70] J. J. Binney and M. Merrifield, *Galactic Astronomy*, published by Princeton University Press, 1998.
- [71] A. M. Green, *Phys. Rev.* **D68** (2003) 023004, [astro-ph/0304446].

- [72] M. C. Smith *et. al.*, *Mon. Not. Roy. Astron. Soc.* **379** (2007) 755–772, [astro-ph/0611671].
- [73] P. Belli, R. Cerulli, N. Fornengo, and S. Scopel, *Phys. Rev.* **D66** (2002) 043503, [hep-ph/0203242].
- [74] A. Bottino, F. Donato, N. Fornengo, and S. Scopel, *Phys. Rev.* **D72** (2005) 083521, [hep-ph/0508270].
- [75] W. M. Yao *et. al.*, **Particle Data Group** Collaboration *J. Phys.* **G33** (2006) 1–1232.
- [76] A. Pukhov, hep-ph/0412191.
- [77] M. A. Shifman, A. I. Vainshtein, and V. I. Zakharov, *Phys. Lett.* **B78** (1978) 443.
- [78] A. Djouadi, J. Kalinowski and M. Spira, *Comput. Phys. Commun.* **108** (1998) 56 [arXiv:hep-ph/9704448].
- [79] A. Bottino, F. Donato, N. Fornengo, and S. Scopel, *Astropart. Phys.* **18** (2002) 205–211, [hep-ph/0111229].
- [80] J. D. Vergados, hep-ph/0601064.
- [81] J. Gasser and H. Leutwyler, *Phys. Rept.* **87** (1982) 77–169.
- [82] M. M. Pavan, I. I. Strakovsky, R. L. Workman, and R. A. Arndt, *PiN Newslett.* **16** (2002) 110–115, [hep-ph/0111066].
- [83] T. P. Cheng, *Phys. Rev.* **D38** (1988) 2869.
- [84] J. Gasser, H. Leutwyler, and M. E. Sainio, *Phys. Lett.* **B253** (1991) 252–259.
- [85] J. Gasser, H. Leutwyler, and M. E. Sainio, *Phys. Lett.* **B253** (1991) 260–264.
- [86] G. K. Mallot, hep-ex/9912040.
- [87] A. Airapetian *et. al.*, **HERMES** Collaboration *Phys. Rev.* **D75** (2007) 012007, [hep-ex/0609039].
- [88] E. S. Ageev *et. al.*, **COMPASS** Collaboration *Phys. Lett.* **B647** (2007) 330–340, [hep-ex/0701014].
- [89] M. V. Polyakov, A. Schafer and O. V. Teryaev, *Phys. Rev. D* **60** (1999) 051502 [arXiv:hep-ph/9812393].
- [90] M. Alekseev *et. al.*, **COMPASS** Collaboration arXiv:0707.4077 [hep-ex].
- [91] A. Airapetian *et. al.*, **HERMES** Collaboration *Phys. Rev.* **D71** (2005) 012003, [hep-ex/0407032].
- [92] S. Aoki, M. Doui, T. Hatsuda, and Y. Kuramashi, *Phys. Rev.* **D56** (1997) 433–436, [hep-lat/9608115].

- [93] D. Dolgov *et. al.*, **LHPC** Collaboration *Phys. Rev.* **D66** (2002) 034506, [[hep-lat/0201021](#)].
- [94] J. Pumplin, D. R. Stump, J. Huston, H. L. Lai, P. Nadolsky and W. K. Tung, *JHEP* **0207** (2002) 012 [[arXiv:hep-ph/0201195](#)].
- [95] A. Djouadi and M. Drees, *Phys. Lett.* **B484** (2000) 183–191, [[hep-ph/0004205](#)].
- [96] B. A. Kniehl and M. Spira, *Z. Phys. C* **69** (1995) 77 [[arXiv:hep-ph/9505225](#)].
- [97] A. Kryjevski, *Phys. Rev. D* **70** (2004) 094028 [[arXiv:hep-ph/0312196](#)].
- [98] G. Bélanger, F. Boudjema, A. Pukhov, and A. Semenov, *Comput. Phys. Commun.* **174** (2006) 577–604, [[hep-ph/0405253](#)].
- [99] P. Skands *et. al.*, *JHEP* **07** (2004) 036, [[hep-ph/0311123](#)].
- [100] J. Engel and P. Vogel, *Phys. Rev.* **D40** (1989) 3132–3135.
- [101] M. Battaglia *et. al.*, *Eur. Phys. J.* **C33** (2004) 273–296, [[hep-ph/0306219](#)].
- [102] E. Brubaker *et. al.*, **Tevatron Electroweak Working Group** Collaboration [hep-ex/0608032](#).
- [103] J. A. Aguilar-Saavedra *et. al.*, *Eur. Phys. J.* **C46** (2006) 43–60, [[hep-ph/0511344](#)].
- [104] A. Djouadi, J.-L. Kneur, and G. Moultaka, *Comput. Phys. Commun.* **176** (2007) 426–455, [[hep-ph/0211331](#)].
- [105] A. Belyaev, private communication.
- [106] P. Gondolo, private communication.
- [107] A. Belyaev, C.-R. Chen, K. Tobe, and C. P. Yuan, *Phys. Rev.* **D74** (2006) 115020, [[hep-ph/0609179](#)].
- [108] G. Bélanger, F. Boudjema, A. Pukhov, and A. Semenov, *Comput. Phys. Commun.* **176** (2007) 367–382, [[hep-ph/0607059](#)].
- [109] G. Bélanger, F. Boudjema, S. Kraml, A. Pukhov, and A. Semenov, *Phys. Rev.* **D73** (2006) 115007, [[hep-ph/0604150](#)].
- [110] C. Hugonie, G. Belanger, and A. Pukhov, [arXiv:0707.0628](#) [[hep-ph](#)].
- [111] G. Bélanger, F. Boudjema, C. Hugonie, A. Pukhov, and A. Semenov, *JCAP* **0509** (2005) 001, [[hep-ph/0505142](#)].
- [112] P. C. Divari, T. S. Kosmas, J. D. Vergados, and L. D. Skouras, *Phys. Rev.* **C61** (2000) 054612.
- [113] J. Engel, M. T. Ressel, I. S. Towner, and W. E. Ormand, *Phys. Rev.* **C52** (1995) 2216–2221, [[hep-ph/9504322](#)].

- [114] V. Dimitrov, J. Engel, and S. Pittel, *Phys. Rev.* **D51** (1995) 291–295, [[hep-ph/9408246](#)].
- [115] J. Engel, S. Pittel, E. Ormand, and P. Vogel, *Phys. Lett.* **B275** (1992) 119–123.
- [116] M. T. Ressel *et. al.*, *Phys. Rev.* **D48** (1993) 5519–5535.
- [117] J. Engel, *Phys. Lett.* **B264** (1991) 114–119.